

DRAFT DISCLAIMER

This contractor draft document was prepared for the U.S. Department of Energy (DOE), but has not undergone programmatic, policy, or publication review, and is provided for information only. The document provides preliminary information that may change based on new information or analysis, and is not intended for publication or wide distribution; it is a lower level contractor document that may or may not directly contribute to a published DOE report.

This document has not undergone technical reviews at the contractor organization, nor has it undergone a DOE policy review. Therefore, the views and opinions of authors expressed may not state or reflect those of the DOE. However, in the interest of the rapid transfer of information, we are providing this document for your information, per your request.

**PRELIMINARY DRAFT
INFORMATION ONLY**

Civilian Radioactive Waste Management System

Management & Operating Contractor

THERMAL TEST PROGRESS REPORT #2

BABEAF000-01717-5700-00001 REV 00

Prepared for:

**U.S. Department of Energy
Yucca Mountain Site Characterization Office
P.O. Box 30307
North Las Vegas, NV 89036-0307**

Prepared by:

**Natural Environment Program Operations
Civilian Radioactive Waste Management System
Management and Operating Contractor
1261 Town Center Drive
Las Vegas, NV 89134-6352**

**Under Contract Number
DE-AC08-91RW0034**

**PRELIMINARY DRAFT
INFORMATION ONLY**

EXECUTIVE SUMMARY

This Thermal Test Progress Report # 2 is the second of a series of informal reports intended to communicate the progress of the in-situ thermal tests. The progress reports are prepared and distributed every three months or so.

The Single Heater Test (SHT), the Large Block Test (LBT) and the Drift Scale Test (DST) are the three components of the current in-situ thermal testing program at Yucca Mountain.

The Single Heater Test Final Report, a level 3 deliverable, is currently in preparation. It is in QAP-SIII-2Q review at this time and is scheduled to go into final QC Check Review next week. The report is expected to be submitted to DOE toward the end of May, 1999. The outcome of the Single Heater Test, as given in the final report, is covered in Section 2.

The Large Block Test is discussed in Section 3. The heating and cooling phases of the LBT are complete and measurements of temperature and moisture content of the block have been terminated. Overcoring for post-test characterization of the block has been completed. Laboratory testing, modeling and analysis will continue over the next several months and the final report is expected to be completed in August, 1999.

The Drift Scale Test is covered in Section 4. The heating phase of the test is in its 17th month now. It is expected to extend approximately another three years. Measurements of various kinds being made in the DST are presented and discussed in Section 4.

CONTENTS

	Page
1. INTRODUCTION	1-1
2. SINGLE HEATER TEST	2-1
2.1 Single Heater Test Final Report	2-1
2.2 Outcome of Single Heater Test	2-1
2.3 Long Term Measurements	2-4
3. LARGE BLOCK TEST	3-1
4. DRIFT SCALE TEST	4-1
4.1 Heater Power and Temperature Data	4-1
4.2 Mechanical Measurements	4-17
4.3 Active Pneumatic Testing and Passive Monitoring	4-19
4.4 ERT Measurements	4-23
4.5 GPR Measurements	4-33
4.6 Neutron Logging Measurements	4-36
4.7 Gas Sampling and Analysis	4-40
4.8 Water Sampling and Analysis	4-44
4.9 Acoustic Emission/Microseismic Monitoring	4-50
4.10 Video Imaging Inside the Heated Drift	4-52
4.11 Heat Loss Through the DST Bulkhead	4-53
4.12 Thermo-hydrologic Analysis of the DST	4-56
4.13 Thermo-hydro-chemical Analysis of the DST	4-62
4.14 Heating Plan	4-80
4.15 DECOVALEX III	4-81

1. INTRODUCTION

Two types of formal reports have generally been employed to date to present and discuss results of the in-situ thermal tests. These are the level 4 deliverable reports and the level 3 deliverable reports. The level 4 or the more numerous kind of reports cover one or a few aspects/subjects associated with a particular test such as the Single Heater Test or the Drift Scale Test. Usually, they cover all the work performed by a teammate organization with respect to a specific test. The level 3 reports, which are fewer, are intended to document in a comprehensive and integrated fashion all aspects of a particular test over a specific period of time. The contents of a level 4 report are incorporated in a subsequent level 3 report associated with the test. Both level 4 and level 3 reports are subject to rigorous guidelines of product quality in terms of reference citations, data presentations and interpretations, to ensure traceability, transparency and QA pedigree of information presented and discussed.

Because of the unavoidable overlap/duplication of efforts in preparing both the level 3 and level 4 reports and in order to streamline the process so that resource utilization is optimized, it has been decided to prepare only integrated level 3 reports for the thermal tests starting in FY99. There will still be some level 4 deliverables from each teammate organization comprising of semi-annual data submittals to the technical database. However, there will be no formal level 4 reports. Elimination of the level 4 reports is not expected to adversely impact the communication within the thermal test team. Such communication is continuously ongoing and is greatly enhanced by the workshops every three months. Since the level 3 reports will be approximately 12 months apart, the absence of the more frequent level 4 reports may cause a gap in others' awareness about the progress of the thermal tests. To avoid such a situation, a series of informal reports, covering all aspects of the thermal tests, will be prepared and distributed. This report, designated Thermal Test Progress Report #2, is the second of a series of informal reports which will be prepared shortly after each quarterly workshop to ensure wider dissemination of information on the progress of the thermal tests. Although, much of the information in the progress reports will be derived from the preceding workshop, these reports will not be limited to a summary of the workshop presentations and discussions. Any information, relevant to the in-situ thermal tests, available at the time of publication of a progress report will be included and discussed in it.

This Thermal Test Progress Report #2 is prepared following the seventh workshop held at Berkeley National Laboratory in January, 1999.

2. SINGLE HEATER TEST

2.1 Single Heater Test Final Report

The Single Heater Test Final Report, a level 3 deliverable, is currently in preparation. It is in QAP-SIII-2Q review at this time and is scheduled to go into final QC Check Review next week. The report is expected to be submitted to DOE toward the end of May, 1999.

2.2 Outcome of Single Heater Test

The outcome of the SHT, as given in the current draft of the final report, is recapitulated herein :

- Conduction is the dominant heat transfer mechanism in the Single Heater Test block, although the pore water in the rock plays a role via the convection mode, both in the liquid and gas phases. It is important to take this into account in modeling, to correctly predict the effects of heating the rock, such as the distribution of temperature increase and movement of water.
- Based on locations of increased and decreased saturations as monitored in the test by electrical resistivity tomography, neutron logging, and ground penetrating radar, and such locations predicted by the models, as well as comparisons of the predicted and measured temperatures, the dual permeability model is considered to be more effective than the equivalent continuum model in simulating the thermal-hydrologic processes in the Single Heater Test block.
- Electrical resistivity tomography and ground penetrating radar measurements in the Single Heater Test tend to suggest, as does dual permeability modeling, that rock moisture mobilized by heating drains, on condensation, by gravity via fractures to below the heated region rather than stay perched above it. This is an important finding with respect to a hot repository, and various observations in the Drift Scale Test so far are bearing this out.
- Pneumatic measurements in the Single Heater Test indicate that air-permeability in certain regions of the test block some distance away from the heater, decreased by a factor of 2 to 5 during the heating phase due to filling of fractures by the condensation of mobilized moisture. Permeability recovered when the heating stopped, as the supply of mobilized moisture ended and liquid water drained down the fractures by gravity.
- Electrical resistivity tomography and neutron logging measurements show good agreement with each other in tracking the growth of the drying regions. The transition from drying to wetting regions observed by neutron logs in boreholes 22 and 23 matches well with the drying/wetting transition derived from electrical resistivity tomography measurements.

- Temperature measurements in the neutron boreholes indicate that drying of the rock begins to occur well before the boiling temperature of 95°C is reached. Drying may occur in regions where the temperature is 60°C or more.
- The coefficient of thermal expansion of the rockmass below 200°C, as derived from measured displacements and temperatures in the Single Heater Test, is as much as 50 percent less than that measured in the laboratory using small hand samples. This lowering of the coefficient of thermal expansion in the larger scale is considered to be caused by fractures which tend to accommodate a large part of the expansion of the rock due to heating.
- Based on comparative analyses of various sets of predicted temperatures and the measured temperatures, the Single Heater Test indicates that the thermal conductivity of the in situ rock is substantially higher than that of dried rock, because of the moisture in the rock which has a higher thermal conductivity. This difference needs to be taken into account in simulating the thermal-hydrologic process to yield more accurate temperature predictions.
- Chemical analysis of samples of water mobilized by heat in the Single Heater Test and subsequent modeling to recreate the characteristics of this water demonstrated that gas-phase reactions play an important role in the thermal-chemical response of the rock. The slightly depressed pH of the water samples indicates that CO₂ partial pressure in the Single Heater Test have been as much as two orders of magnitude higher than that in ambient atmosphere.
- Interpretive analysis of the chemical compositions of the samples of water from borehole 16 in the context of reaction-transport simulations of the chemical processes in the Single Heater Test, leads to the conclusion that the borehole 16 water resulted from steam condensation in fractures. The mildly acidic character of the water reflects the dissolution of gaseous CO₂ at the time of condensation. The simulations indicate that dissolved carbonate species in matrix water alone is a sufficient source of CO₂ gas to drive the pH down to a mildly acidic range.
- Calcium, gypsum and amorphous silica were found in the posttest mineralogic analyses of the samples from the overcoring of borehole 16. The distribution and textural attribute of these minerals suggest that they formed through evaporation of residual water during the post-heating (cooling phase) of the test.
- Strontium and uranium analyses of the borehole 16 water samples indicate that the concentrations of these cations are not unreasonable compared to that of pore water from these strata, although data on the uranium content of pore water are limited. The ⁸⁷Sr/ ⁸⁶Sr ratio of all the borehole 16 water samples remain essentially constant at ~4.5 which is well within the range measured on pore water from these strata.
- Post-cooling air-permeability measurements show an increase in permeability

ranging from 20 percent to a factor of 3.5 compared to the pre-heating values. Since air-permeability measurements are made over meters of length of borehole and the fluid always seeks the path of least resistance, this increase in permeability is considered to be resulting from the opening of fractures due to heating and/or cooling.

- All the test specimens or coupons of carbon steel left in the two hydrology boreholes before the start of heating underwent various degrees of corrosion. The corrosion products were generally goethite ($-Fe^{+3}O(OH)$) and magnetite (Fe_3O_4). The chloride containing mineral akaganeite ($-Fe^{+3}O(OH,Cl)$) was identified in one coupon.
- The copper tubing protecting the heating elements was found to be covered with oxidation products upon withdrawal after heating and cooling. The oxidation mineralization included tenorite, cuprite, paratacamite and atacamite.
- The performance of the temperature sensors was within expectation; approximately 5 percent of them failed. A small fraction of both thermocouples and resistance temperature detectors failed. None of the thermistors failed.
- The chemical sensors installed in SEAMIST liners and designed to measure various chemical parameters did not function at all because of the unsaturated environment they were in.
- The performance of multiple-point borehole extensometers with high temperature linear variable displacement transducers was superior to the ones with vibrating wire gages; posttest examination and calibration checks indicated that all the high temperature linear variable-displacement transducers were within calibration standards.
- The optical multiple-point borehole extensometers performed as expected; however, the measurements were inferior, in terms of resolution and precision, to those from other systems such as mechanical multiple-point borehole extensometers.
- The ground penetrating radar technique of monitoring the saturation of the rock was found to work as expected. The ability of ground penetrating radar to identify areas of drying was good, while that to identify areas of increased saturation was qualitative. The results of ground penetrating radar and electrical resistivity tomography measurements generally coincided, thereby lending credence to each other.
- The infrared imaging conducted next to the Single Heater Test block failed to detect any heat-mobilized moisture escaping via fractures.
- Last, but not the least, the experiment of having numerous organizational entities

work together in a short period of time and in limited space in fielding the Single Heater Test proved to be effective and successful. The experience made the fielding of the much larger and more complex Drift Scale Test to be completed smoothly the following year.

2.3 Long-term Measurements

How and when the near field rock regains the pore moisture driven away by heating is of considerable interest. The last post-cooling measurements made in both the SHT and the LBT indicated that the dried-out rock had not regained the pore moisture.

The electrodes used for ERT measurements in the SHT are still intact. A proposal is being considered to another set of ERT measurements in the SHT and continue to make bi-annual measurements thereafter in attempt to observe how long it takes the rock to regain its pre-heating saturation.

3 LARGE BLOCK TEST

The heating phase of the Large Block Test began on February 28, 1997 and ended on March 10, 1998 when the heaters were turned off. The cooling of the block was monitored until September 30, 1998 when it was determined that the block had returned to ambient temperature and the Data Acquisition System was turned off. During the heating phase the block was heated from within to reach a temperature of 140⁰C at the heater horizon, and the heat exchanger is used to keep the top temperature at about 60⁰C.

Post-test Characterization

Post-test characterization activities were started in early October 1998 and consist primarily of drilling/coring to provide boreholes and samples for post-test characterization of the block, and laboratory testing and analysis of core samples collected by the drilling/coring activity. In addition, numerical modeling of the hydrologic and geomechanical behavior of the LBT is also being conducted.

Drilling/Coring Activities

The post-test drilling and coring activities include drilling of nineteen new boreholes and one overcore of an existing borehole. These holes are arranged as shown in Figure 3-1, which shows that two vertical fans of boreholes are to be drilled, one from the North side of the block, and the other from the west side. The holes forming the fans are size HQ, which produces a 4 in. diameter hole, and 2.5 in. diameter core. All holes were drilled dry. This drilling pattern provides a moderately high density of sampling in two perpendicular vertical planes in the block. The post-test holes are designed to intersect several of the instrumentation holes in the block. This will provide samples of grout as well as rock for evaluation.

Figure 3-1 also shows the location of the overcore hole. This will be a 10 inch over core of heater hole #4. The purpose of this hole is to provide samples of rock which experienced the highest temperature over the longest time period. Drilling of the post-test characterization holes started on Nov. 1, 1998 and was completed by February 19, 1999. All holes were successfully drilled, and core recovery was high, generally over 90%. Core samples were logged, videologged, wrapped in plastic, sealed in lexan tubes, then sealed in core-protect bags. The core samples are currently at the Sample Management Facility. Analysis of the core will start in March 1999.

Video logs of the new boreholes were taken after the drilling was completed. These video logs will be used to provide new information on the location of fractures in the block. The fracture data from these logs will be added to the existing fracture data base in order to improve the fracture model of the block. These logs will also provide information on the condition of fractures and on the extent of fracture filling associated with grouting of the instrumentation holes.

Laboratory Testing/Analysis of Post-test Samples

A series of laboratory measurements, tests and analyses have been planned to characterize the post-test core samples. These include the following.

- Physical properties such as density, porosity, moisture content.
- Mechanical properties including uniaxial compressive strength and Young's modulus.
- x-ray Diffraction (XRD) analysis to determine mineral content of the matrix material.
- Examination of fracture surfaces using Scanning Electron Microscopy (SEM) to determine type and amount of secondary mineralization that may be associated with hydrothermal processes.

For each of these characterization activities, samples will be selected and prepared from the post-test core from the high temperature, dry out, boiling and wetting zones. In addition, simulations of the LBT are underway using both the NUFT thermohydrological code and the 3-DEC discrete element thermomechanical code. Work has also started on a report documenting the LBT.

LBT post-test boreholes

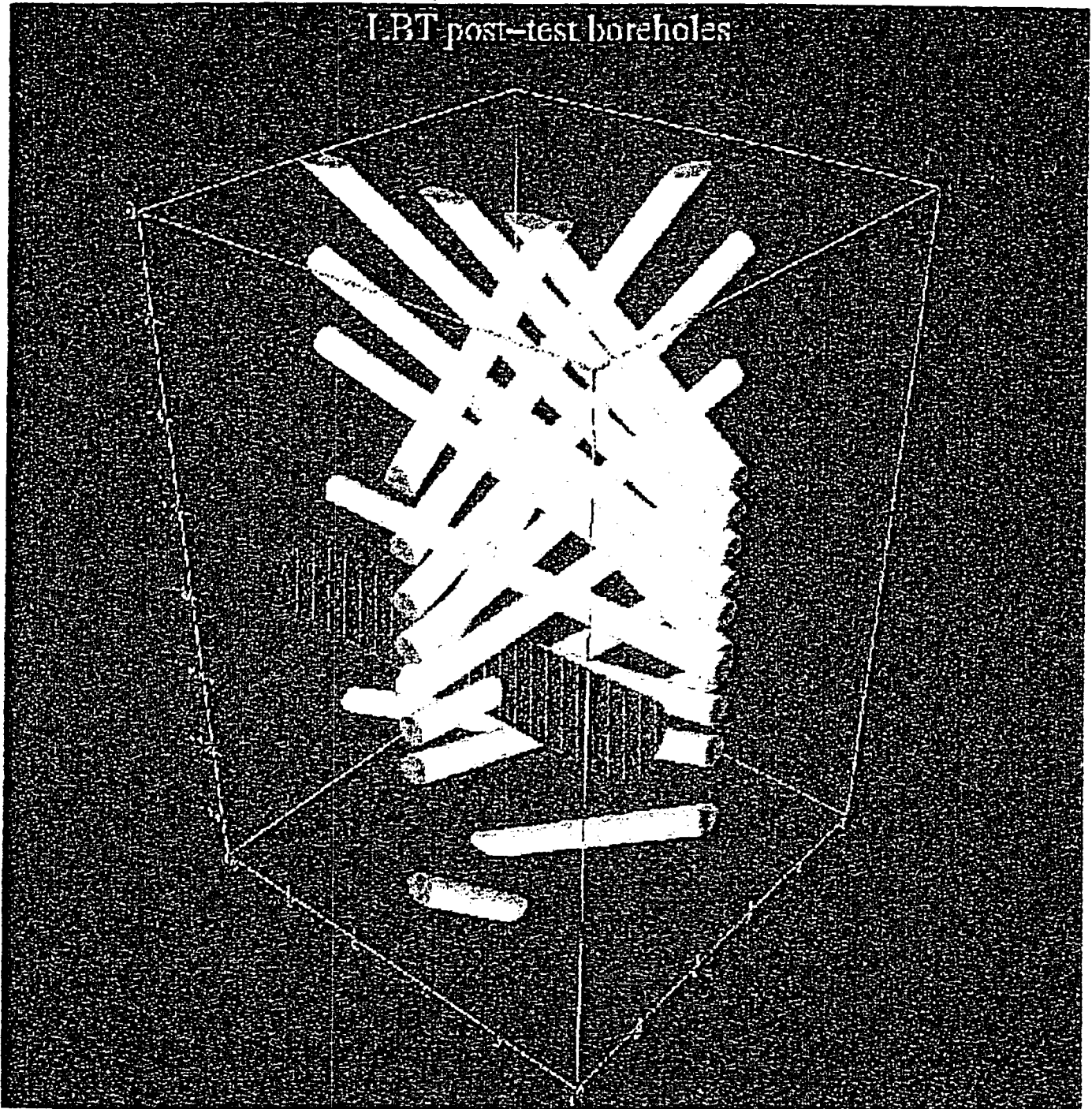


Figure 3-1. Schematic locations of post-test holes drilled in the Large Block Test as viewed from the North West corner of the block. All holes were drilled dry and were continuously core

4.1 Heater Power and Temperature Data

The heater power and temperature data from the Drift Scale Test from the start of heating in December 1997 to December 31, 1998 are presented and discussed in this section.

Heater Power

Figure 4.1-1 illustrates the power being supplied to all of the wing heaters and all of the canister heaters. These total power data are Q measurements. The power being supplied to individual canister heaters are illustrated in Figure 4.1-2. These individual heater power data are not Q measurements.

The wing heater power was fairly constant up until about day 185 (6/6/1998), when it dropped a few percent. This was a result of the loss of power to the inner and outer elements of wing heater 29. On day 211 (7/3/1998) the outer element of wing heater 26 failed. The power distribution to individual wing heater elements on day 393 (9/30/1998) is illustrated in Figure 4.1-3.

The canister heater power decreased from about 53 kW at the beginning of the test to about 51 kW on day 244 (8/4/1998), a drop of about 2%. From day 244 to 270 (8/30/1998) the power increased to about 53.5 kW. This increase is likely due to changes in the ventilation system just outside the Heated Drift, which were implemented on 8/4/1998. These changes resulted in increased airflow near the cables supplying power to the canister heaters. This increased airflow likely cooled the cables, thereby decreasing the cable resistance. Decreased resistance increased the current flow in the heater circuit, thereby increasing the power to the heaters. Both the wing heater and canister heater power have been stable for the last three months of the test.

Temperatures Inside The Heated Drift

Figures 4.1-4, 4.1-5, and 4.1-6 illustrate the temperatures on the canister heaters, in the air in the Heated Drift and on the walls of the Heated Drift, respectively. By day 393 (12/31/1998) the canisters had reached temperatures as high as 170 °C while the air and wall surface temperatures were in the 140 to 150 °C range. For each of these three data sets, the temperatures started out at about 30 °C just prior to the start of the test. When the heaters were activated, the temperatures rose very rapidly at first, but then the rate of increase of temperature decreased with time up until about day 130 (4/12/1998). From day 130 to day 239 (7/30/1998) the temperatures increased nearly linearly. The reason the rate of temperature increase stabilized is likely due to the presence of the wing heaters; without them, the rate of temperature increase would likely have continued to decrease. On day 239, there was a drop in the canister, air and surface temperatures of about 5 °C. This resulted from changes to the air ventilation system on the cool side of the bulkhead which caused more cool air to be

circulated onto the surface of the bulkhead. For approximately 5 days, cool, ambient air was forced into the Heated Drift through a hole in the bulkhead. When the hole was closed, the temperatures started to increase again. It is interesting to note that after the hole was sealed the rate of temperature increase, while still nearly constant, appears to be slightly less than the rate of temperature increase prior to the incident with the hole. This likely reflects an increase in heat flux out of the bulkhead as a result of the increase in the vigor of the ventilation system on the cool side of the bulkhead. On about day 309 (10/8/1998) the ventilation system on the cool side of the bulkhead was modified in a manner that reduced the air flow near the bulkhead. This change resulted in less heat flux through the bulkhead and the canister, air and rock wall temperatures all increased slightly but noticeably. By day 393 (12/31/1998), the middle part of the drift was about 6 to 8 °C warmer than the ends (Figures 4.1-7 and 4.1-8).

Figure 4.1-9 illustrates the air pressure and humidity measured inside the Heated Drift. These measurements are correlated. When the air pressure increases, relatively dry air from outside the Heated Drift is forced into the drift decreasing the humidity. During the time that outside air was being forced into the drift through the hole in the bulkhead there was a pronounced decrease in humidity in the Heated Drift, but no appreciable change in air pressure,.

Figure 4.1-10 illustrates the temperatures recorded by the temperature sensors mounted on the hot side of the thermal bulkhead. The pronounced changes in the temperature distribution on the bulkhead which occurred on day 239 and on day 309 were caused by changes in the thermal insulation on the outside of the bulkhead and in the ventilation system just outside the drift.

Rock Temperatures

Figure 4.1-11 illustrates temperature contours on a vertical plane that is perpendicular to the axis of the drift and which intersects the drift at approximately its midpoint ($Y = 23$ m). The dots indicate the locations of the temperature sensors grouted into eight boreholes radiating out from the drift at this location. The contours in Figure 11 honor the data measured at these locations after 12 months of heating (12/3/1998). The warmest temperatures are measured near the wing heaters and surrounding the top of the Heated Drift. The region immediately below the drift is slightly cooler than the top of the drift because of the insulating effect of the concrete invert in the drift.

Figure 4.1-12 shows the temperatures observed after 393 days of heating (12/31/1998) in the four horizontal boreholes emanating from the Heated Drift. The data indicate that the rock adjacent to the wing heaters is warmer than the rock near the Heated Drift. This is because of the higher power output of the wing heaters as compared to the canister heaters in the drift. The temperatures near the wing heaters show two pronounced "humps", which correspond to the locations of the two wing heater elements deployed in each borehole. The data from the left side of the drift at $Y=12$ meters do not exhibit a noticeable "hump" associated with the outer wing heater since this hole is located midway between wing heaters 6 and 7 and the outer

heating element of wing heater 7 is operating at only about 75% power. Three of the four temperature profiles exhibit a slight shoulder about 14 meters from the drift at a temperature corresponding to the boiling point of water. These are manifestations of a region of rock where water in the pores of the rock is boiling.

Figure 4.1-13 shows the temperatures measured in borehole 172 which is located at Y = 39 meters and which extends downward from heated drift at an angle of approximately 45° from the vertical. Note the isothermal region which extends from about 2 to 4 meters from the drift wall where the temperature is approximately constant at about 97 °C. In this region, water in pores of the rock is boiling and liquid water and steam coexist in the rock.

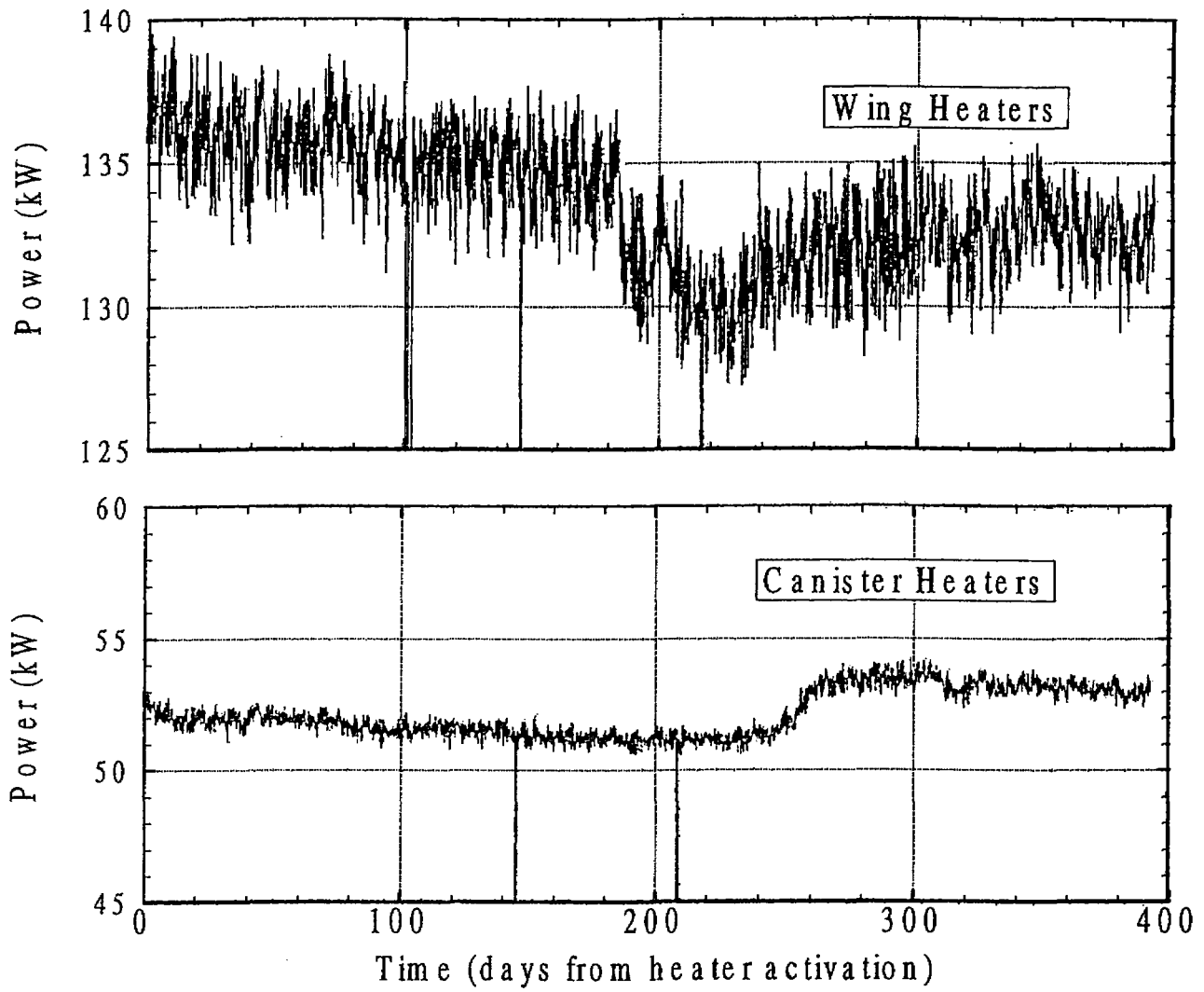


Figure 4.1-1 Total power measurements (Q) for the Wing Heaters and Canister Heaters.

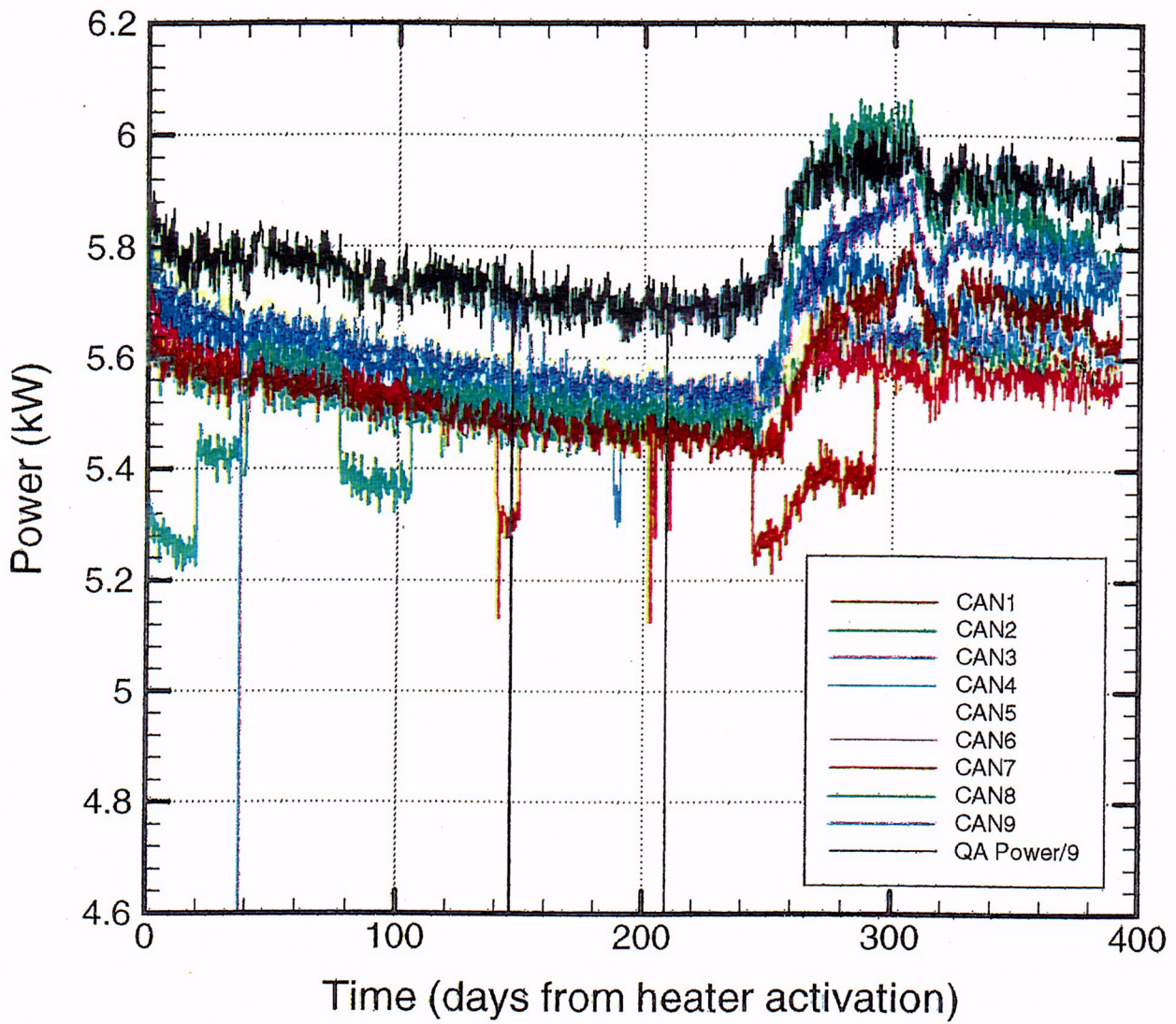


Figure 4.1-2 Power (not Q) for each of the Canister Heaters..

021

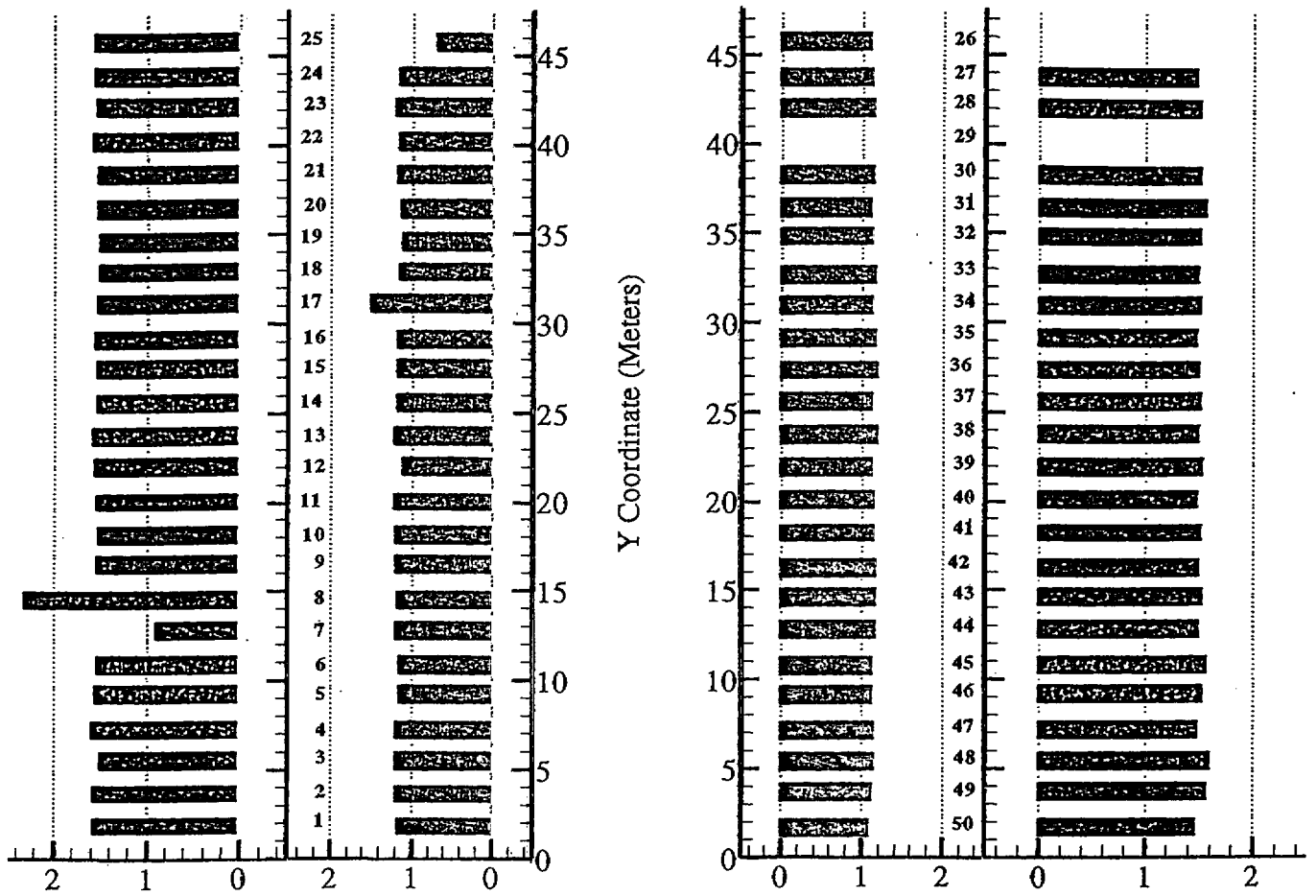


Figure 4.1-3 Power distribution (not Q) to individual wing heater elements on day 393.

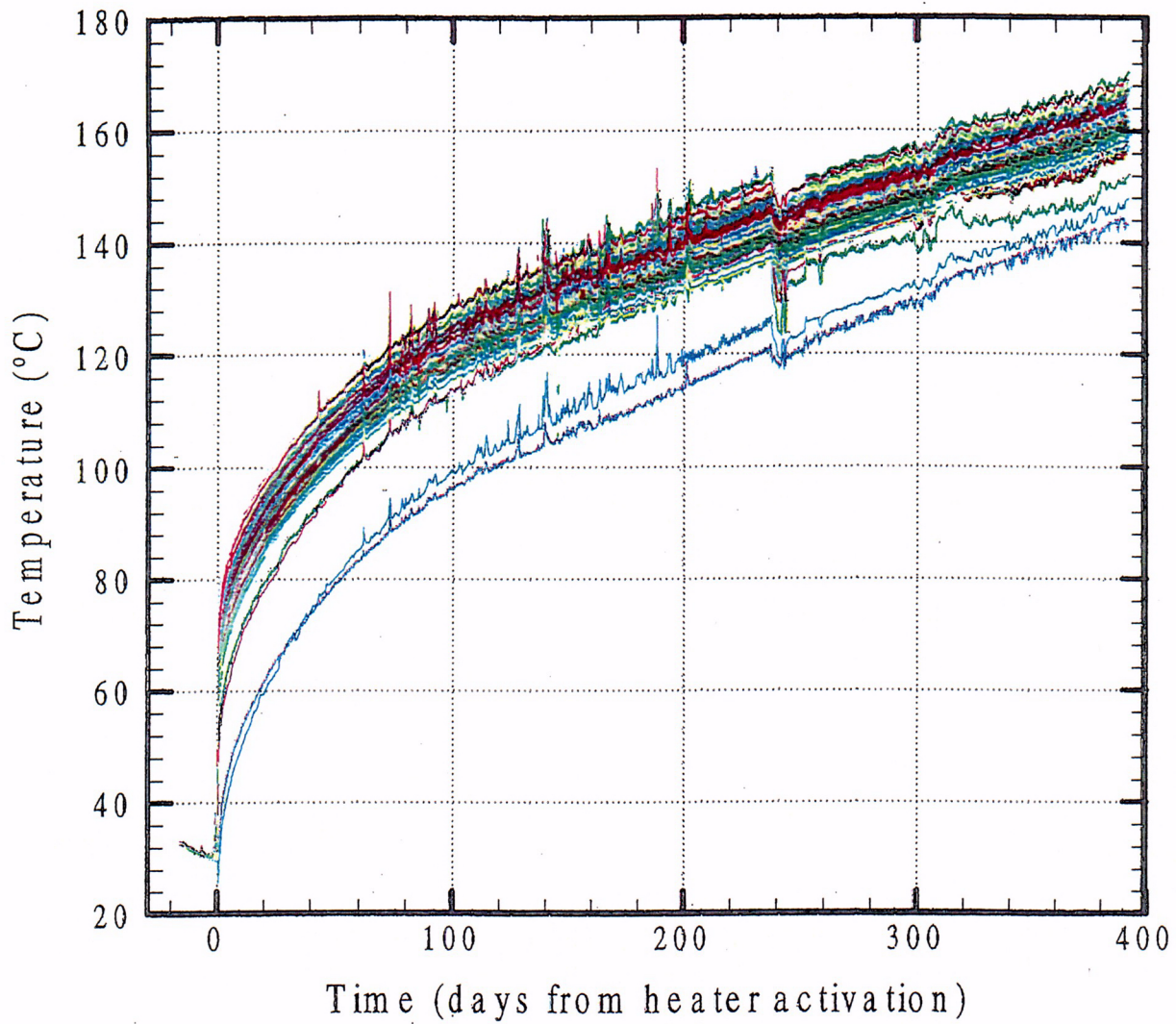


Figure 4.1-4 Temperatures on the canister heaters.

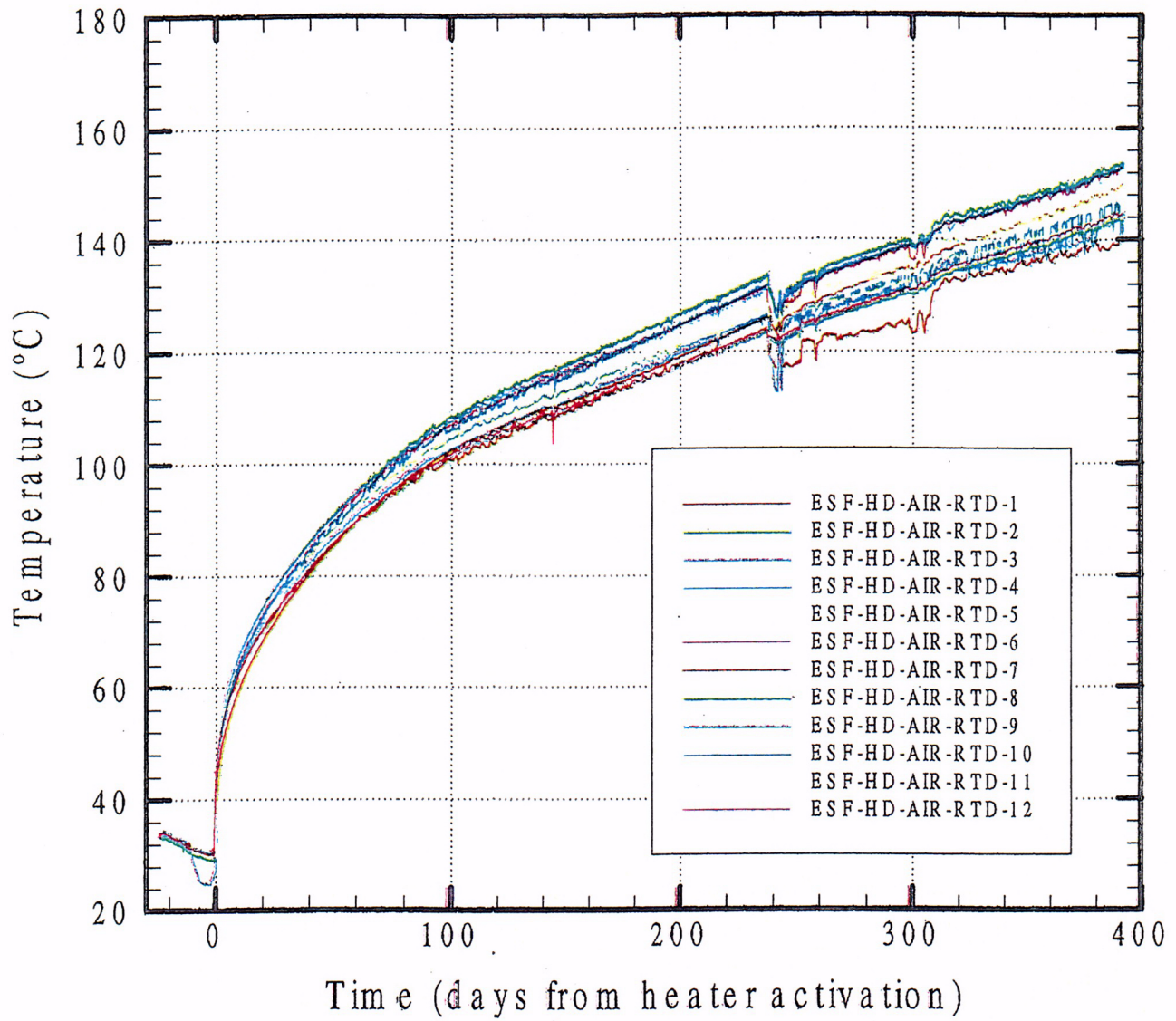


Figure 4.1-5 Temperatures in the air in the Heated Drift.

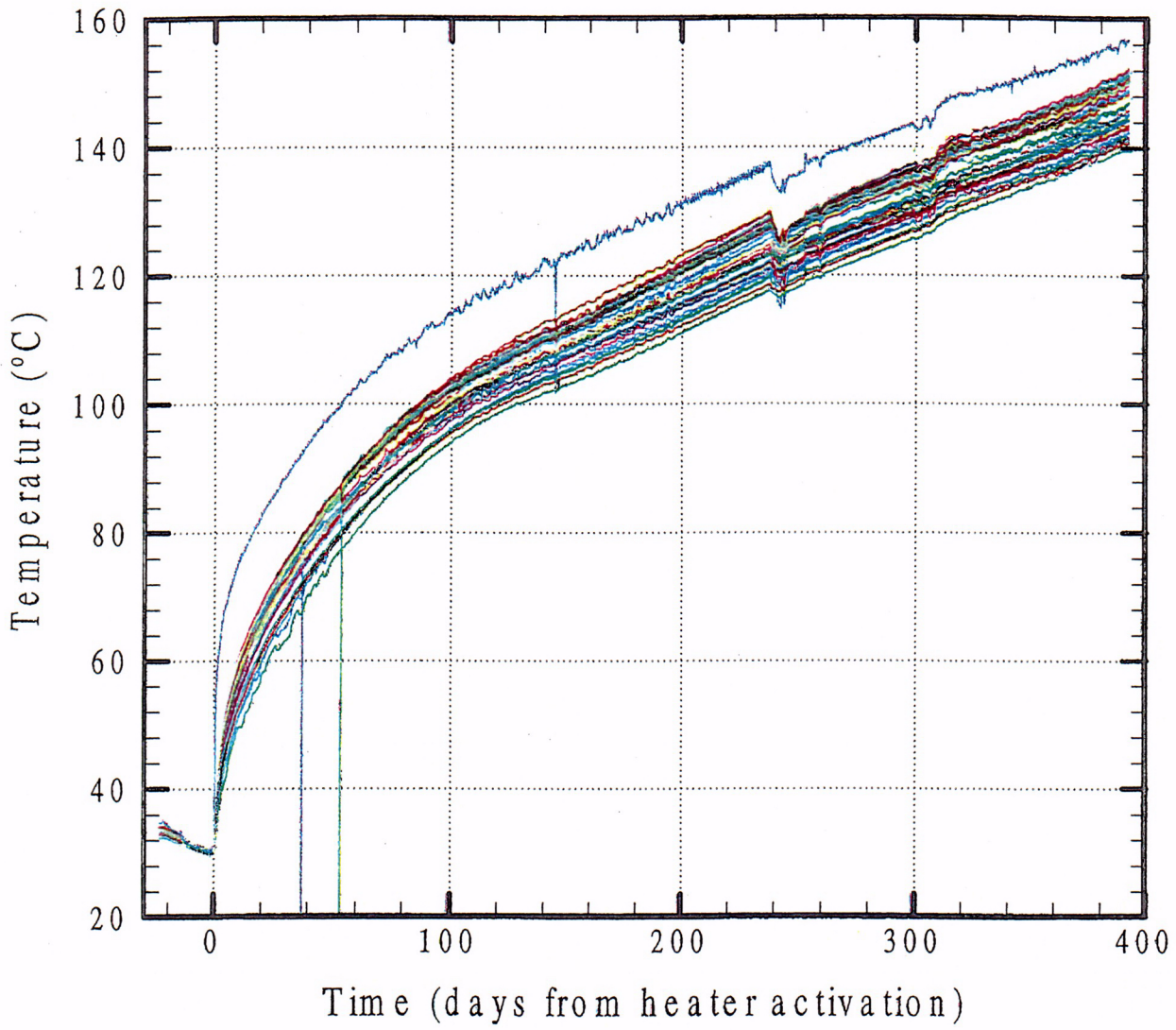


Figure 4.1-6 Temperatures on the walls of the Heated Drift.

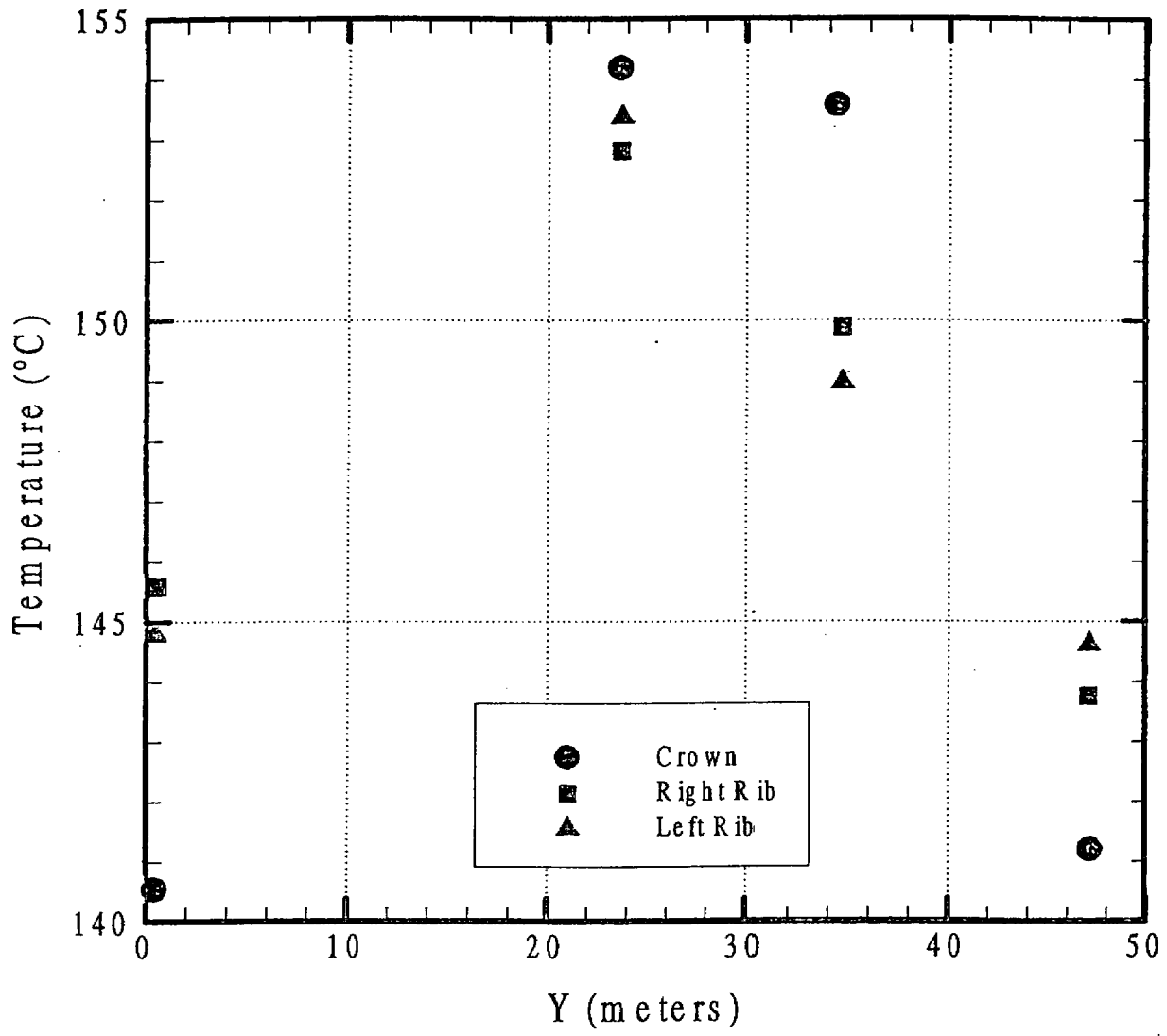


Figure 4.1-7 Temperatures on the walls of the Heated Drift on day 393.

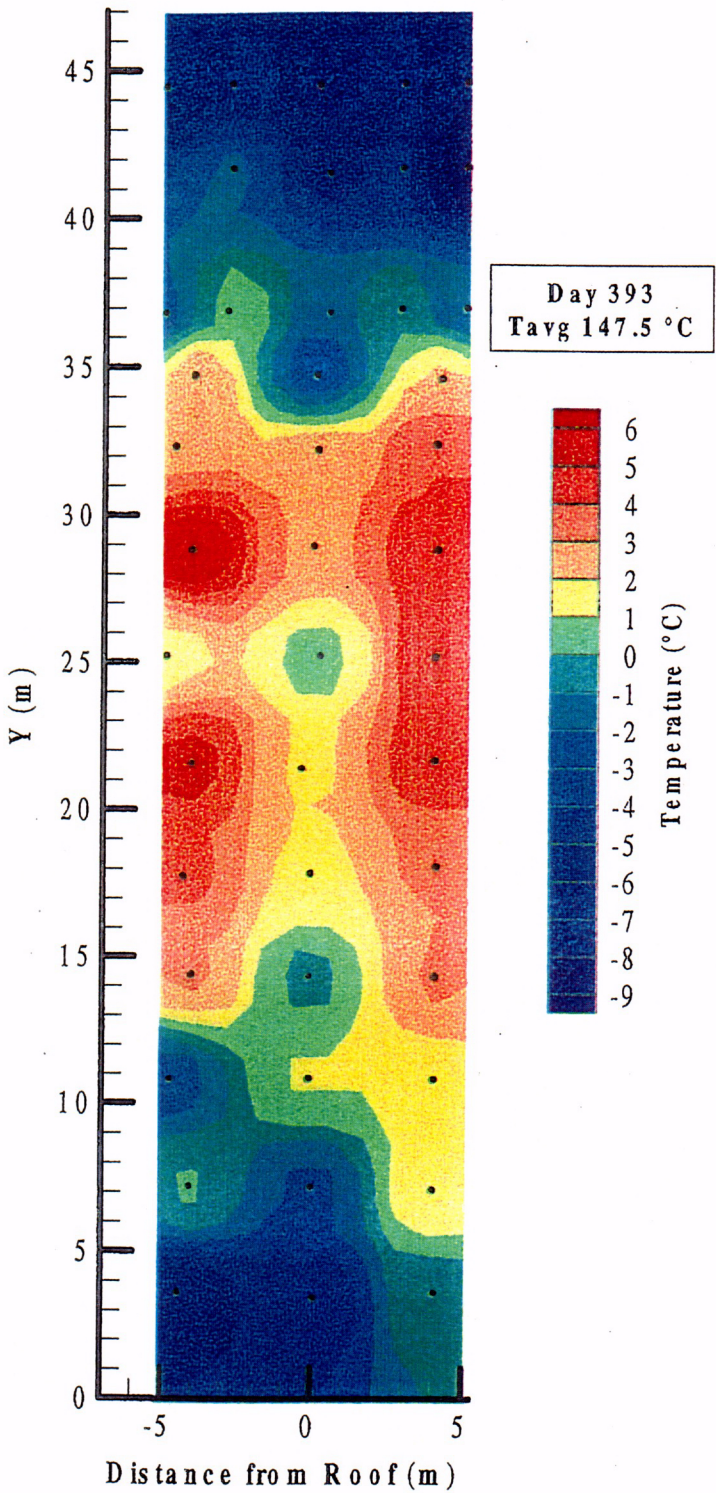


Figure 4.1-8 Contoured temperatures of the wall of the Heated Drift after 393 days of heating.

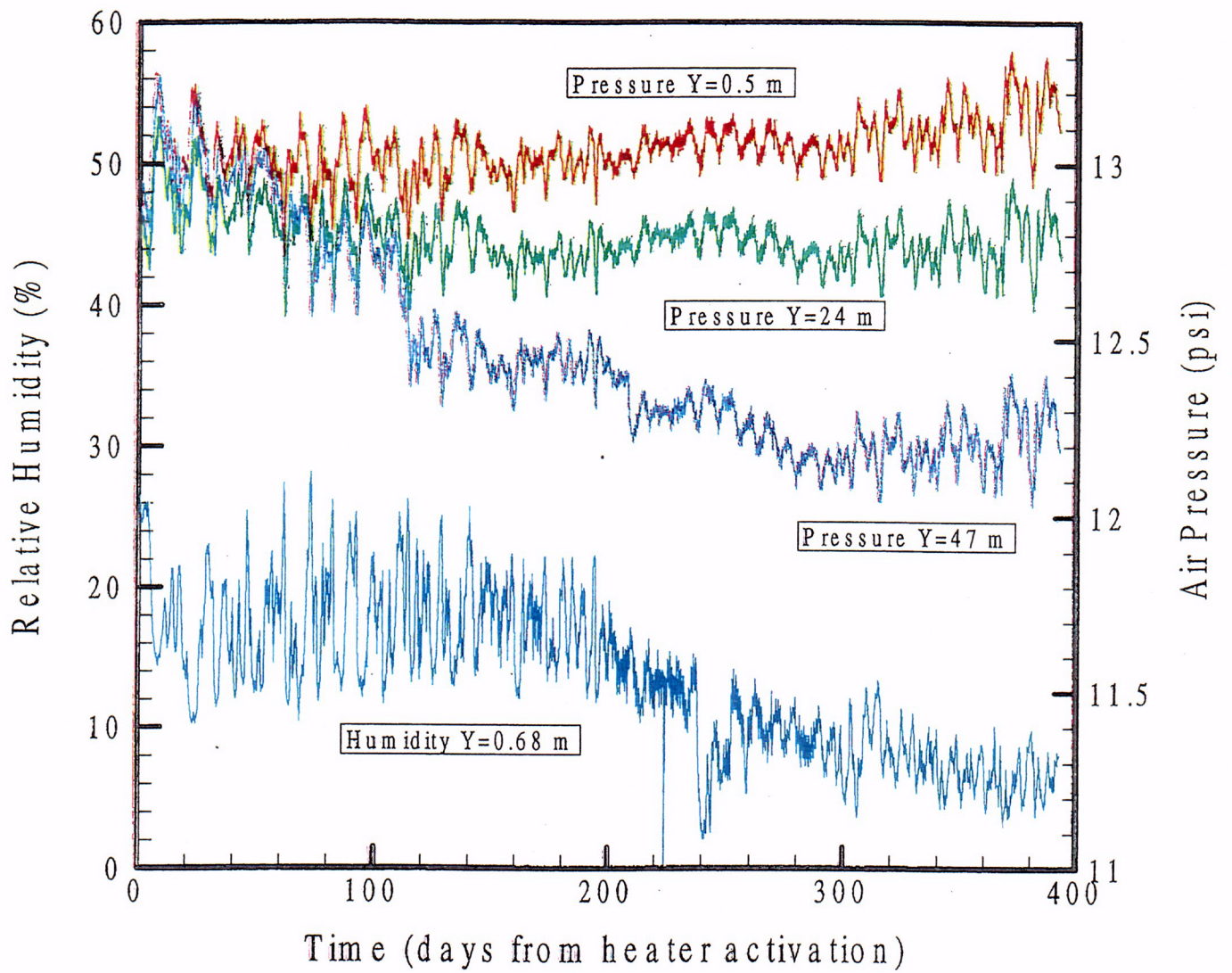


Figure 4.1-9 Relative humidity and air pressure inside the Heated Drift.

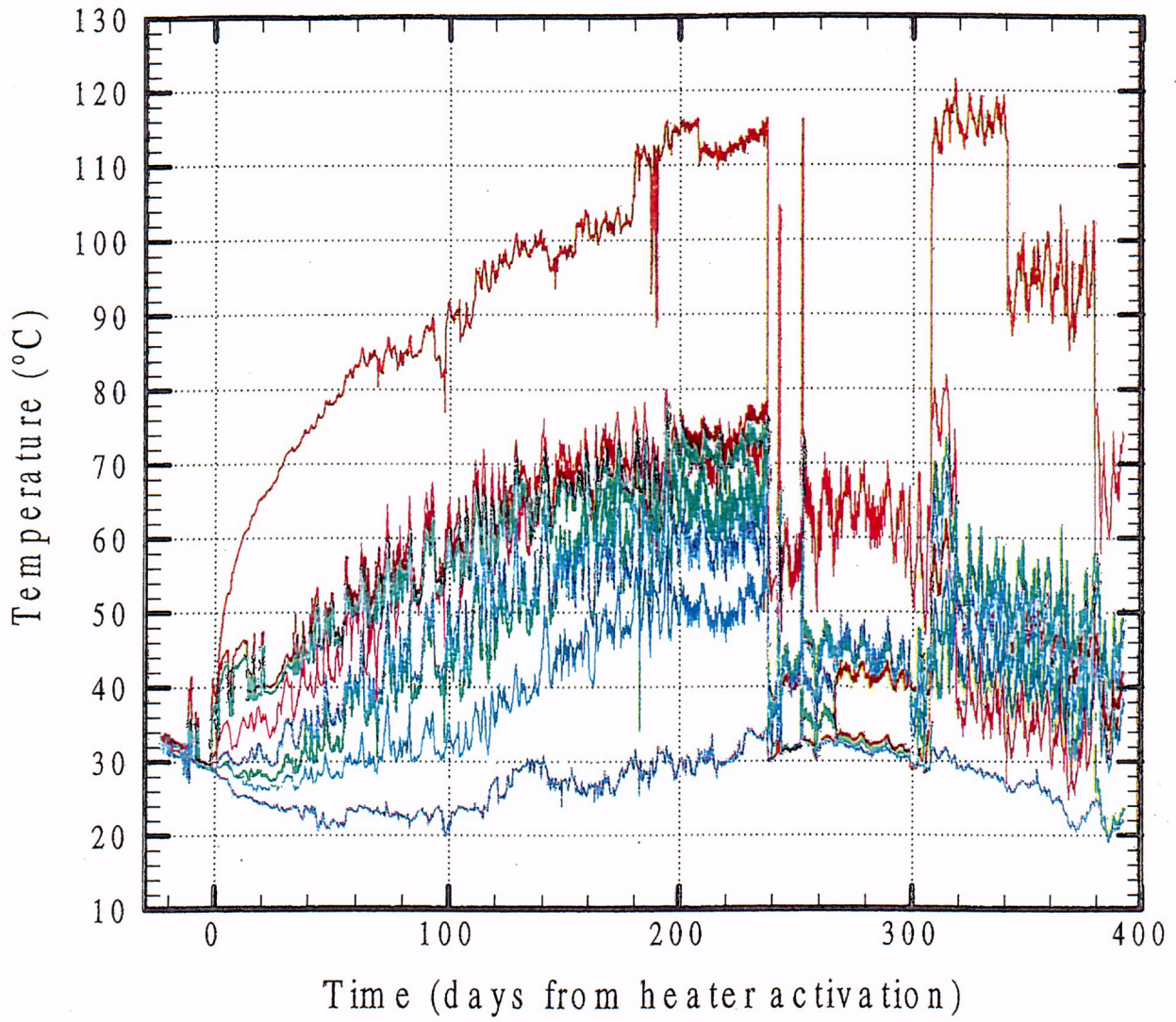


Figure 4.1-10 Temperatures measured on the hot side of the bulkhead.

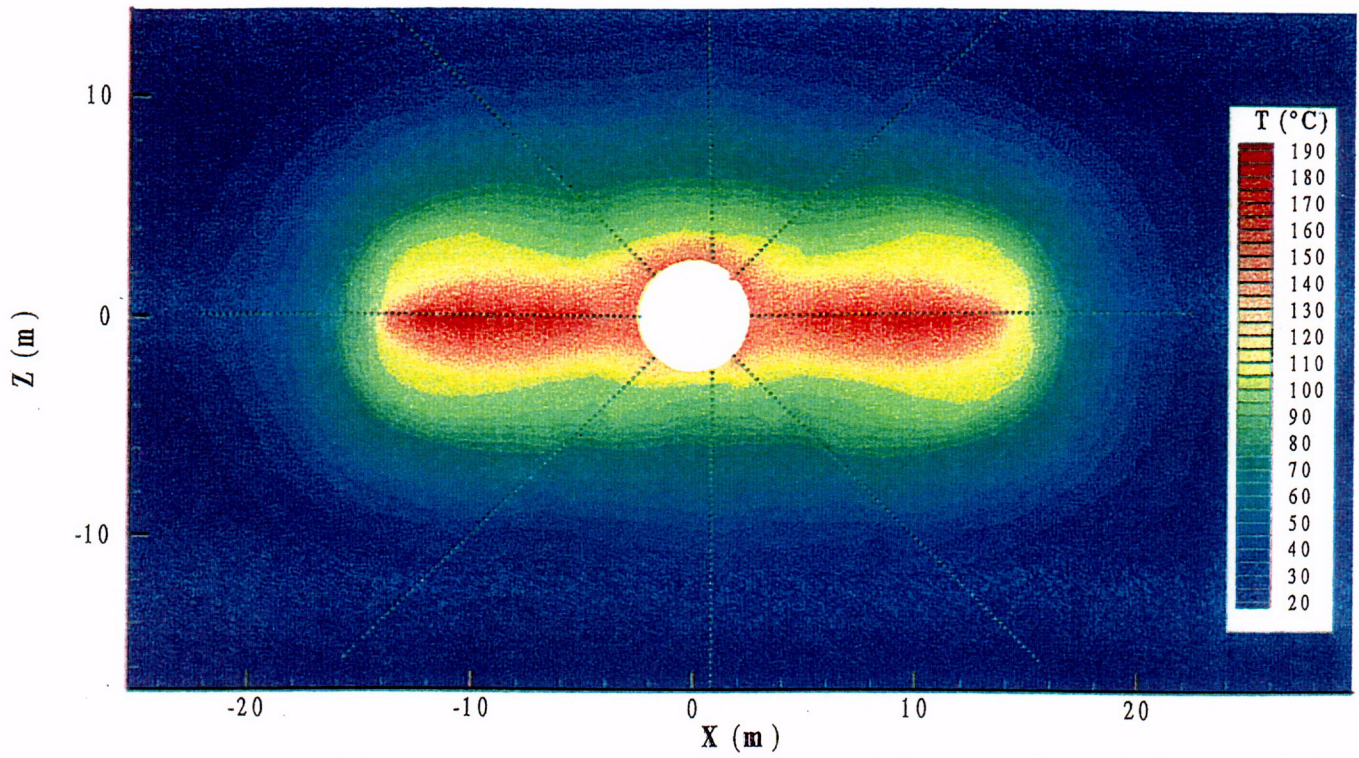


Figure 4.1-11 Temperature contours on the vertical cross section at $Y = 23$ meters after one year of heating.

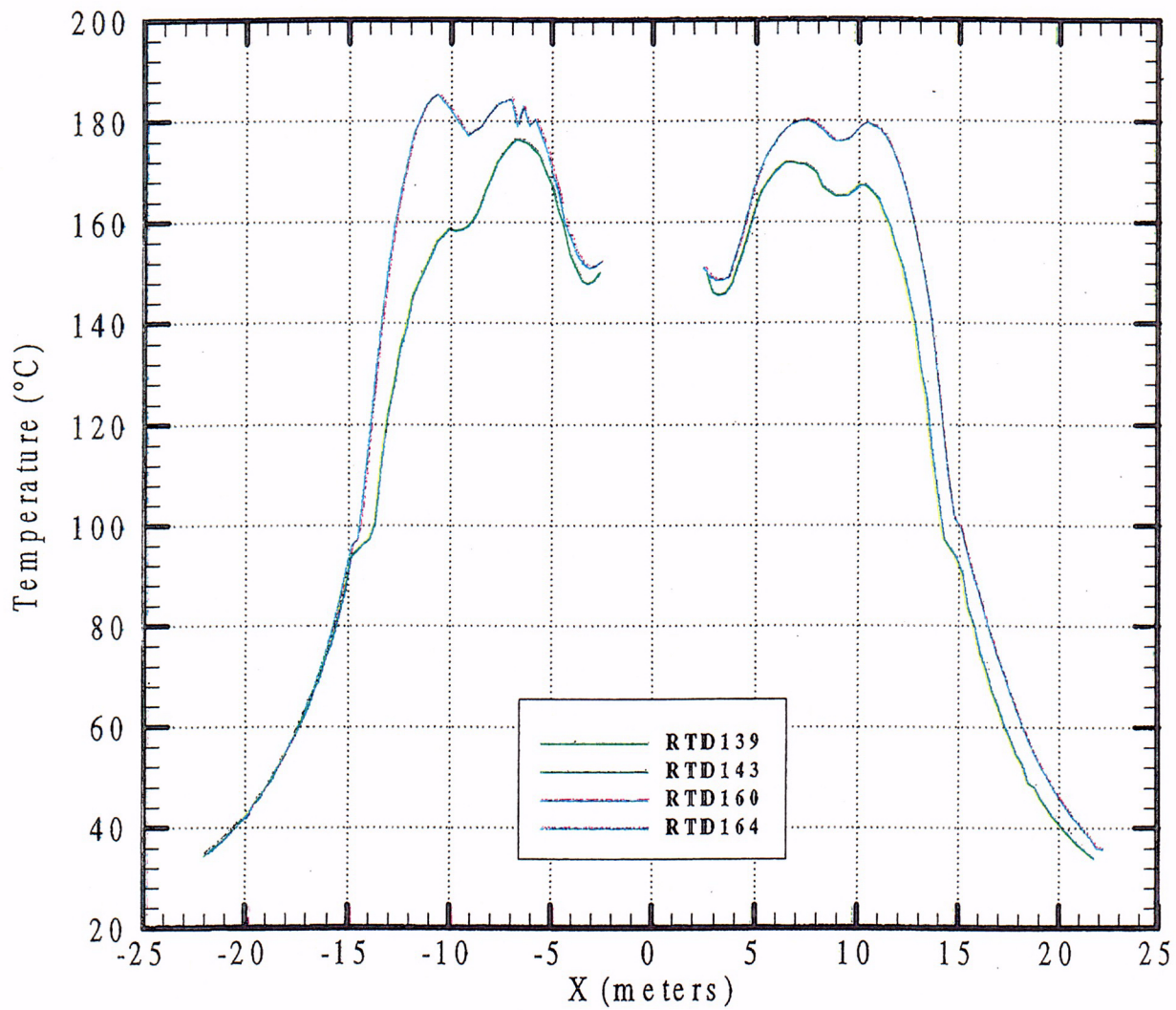


Figure 4.1-12 Temperatures in four horizontal boreholes emanating from the Heated Drift.

Temperatures in Borehole RTD-172 After 393 Days of Heating

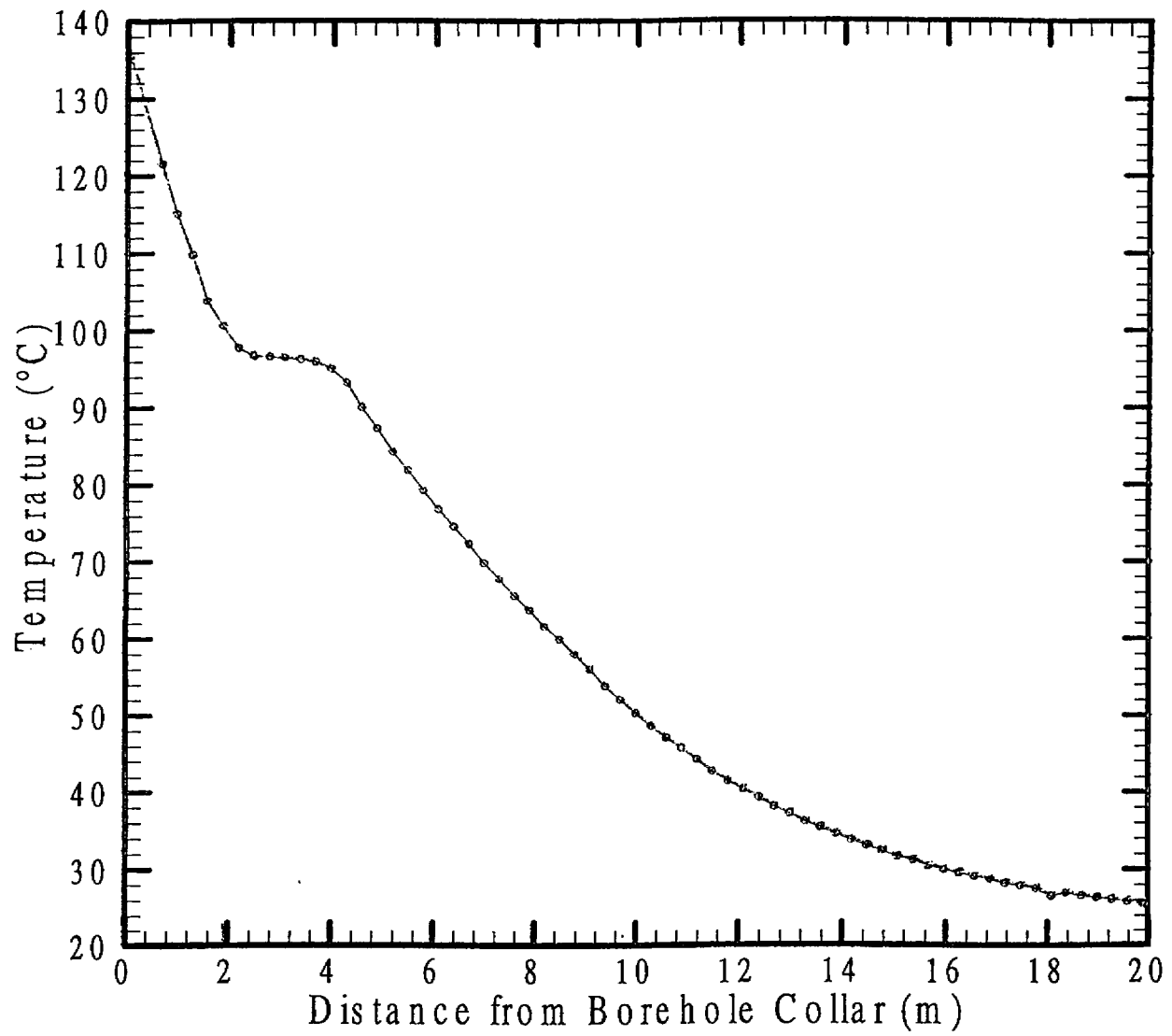


Figure 4.1-13 Temperatures in borehole RTD0172 after 393 days of heating.

4.2 Mechanical Measurements

This short report discusses new events and trends associated with the 4th quarter Drift Scale Test thermal and mechanical data (from 9/1/1998 through 12/31/1998). The discussion here follows on to that of the previous data in the SNL report "Drift Scale Test Draft Status Report #1: Evaluation and Comparative Analysis of the Drift Scale Test Thermal and Thermomechanical Data (Results of 12/3/1997 Through 5/31/1998)" dated July 15, 1998.

Thermal Data

The maximum temperature in the Heated Drift and on its walls (disregarding surface thermocouple SURF-TC-39, which has been anomalous since the initiation of the heaters) as of 12/31/1998 (393 days of heating) was measured to be 149°C. No new anomalies in the drift and surface temperature measurements were observed during the latest time period.

Mechanical Data

The behavior exhibited thus far by the MPBXs continues to be similar to the elastic model predictions, with the exception of MPBX-14, which demonstrates separation between the invert and liner. MPBX-14 indicates de-bonding of the invert from the liner, with a separation as much as 7 mm. The deepest anchor (Anchor #4) for the MPBXs is progressing toward having the largest displacement from the collar. Most of the MPBX sensors are working well; however, MPBX-5, -7, and -11 have gone totally bad, and MPBX-3, -6, and -14 have gotten progressively noisier during the 4th quarter.

The data shows little evidence of non-elastic behavior in terms of specific events or reversals of trends. However, the magnitudes of displacement are somewhat higher than those predicted by elastic analyses using intact rock mechanical properties ($E=37$ GPa, SHT intact rock thermal expansion coefficients), particularly for the closest anchors (1 and 2). This may be indicative of joint deformation behavior near the drift wall, perhaps due to enhanced fracturing near the surface due to mining. A similar phenomenon was observed for the Single Heater Test when comparing elastic and compliant joint predictions to the test data; the compliant joint model predicted higher displacements that were more consistent with the data. SNL is initiating new compliant joint analyses to evaluate the DST MPBX data.

Due to a problem with the revision of the scan software done on August 4th, the CDEX-1 and CDEX-2 data were not read properly by the DCS for the interval from 8/4/1998 until 9/25/1998. The raw data and Q Engineering readings do not exist for these sensors during this interval. After 9/25/1998 the readings are done the normal manner.

The strain gages placed on the concrete liner and on unconstrained concrete samples in the Heated Drift continue to show the combined effects of thermal expansion,

dehydration-induced shrinkage, and mechanical stress imposed by the interaction of the concrete with the heated rock surrounding the drift. The results from the strain gages on the unconstrained samples exhibit behavior indicative of drying shrinkage due to dehydration, a phenomenon seen elsewhere in engineering literature. All of the strain gages on the liner surface are in extension by the end of the 4th quarter due to combined thermal and mechanical effects. The mechanical component of the circumferential strain gages on the liner consistently show that the crown of the liner is in compression while the rest of the liner experiences smaller magnitudes of compression and tension.

Thermal expansion coefficients for $T > 96^{\circ}\text{C}$ have been estimated for the unconstrained coupons. Three of the coupons have a thermal expansion coefficient of $\sim 12 \mu\text{strain}/^{\circ}\text{C}$, whereas the fourth is at $\sim 21 \mu\text{strain}/^{\circ}\text{C}$. There is no apparent correlation of thermal expansion behavior to the type of concrete. There is a possible correlation of behavior due to placement of samples, based on the near linear nature of two of the samples versus a more curved nature to the others. However, documentation of the relative placement of these samples with each other and with the nearby canister heaters is insufficient to determine such a relationship. There is evidence from the axial strain gage data of potential bending due to asymmetric heating of end of drift (WHs 25, 26, 29).

4.3 Active Pneumatic Testing and Passive Monitoring

In the Drift Scale Test the hydrological boreholes consist of three fans of boreholes, referred to as boreholes 57 to 61, 74 to 78, 185 and 186. These twelve boreholes have 46 packers installed. Intervals are referenced by the borehole number followed by the interval number, which ascends from the collar of the borehole to the back of the borehole. Currently two packers are not inflated, packer 77-3 and 186-3. The 44 inflated packers section the twelve boreholes into 44 isolated zones for passive monitoring and active testing.

Passive Monitoring

Passive monitoring of temperature and pressure in each isolated interval is continuing. Two zones show temperatures that have gone above the boiling point of water to date: 60-3 and 77-3. Both boreholes 60 and 77 pass close to the wing heaters, and below the Heated Drift. Passive monitoring shows close tracking between the barometric signal and the pressure fluctuations recorded within each zone. The zones located further from the borehole collars show greater damping of the barometric signal as would be expected.

Active Testing

From November 17 to November 21, 1998 constant mass flux air-permeability tests were conducted in all 44 isolated intervals. Air was injected in each zone for one hour to allow the pressure field to approach a steady-state response and the transient recovery was subsequently monitored. Air-permeability is used to monitor moisture redistribution since increases in liquid saturation will show up as decreases in air-permeability.

The steady-state pressure response was analyzed using the same ellipsoidal flow equation that was used to process previously acquired air-permeability data sets. Figure 1 shows a comparison of air-permeabilities as a ratio to baseline values for zones in the 74 to 78 boreholes cluster showing decreasing air-permeability. As a general trend, intervals located below the wing heaters and the Heated Drift show the greatest decrease in air-permeability, with zones located above the heaters also showing a steady decrease in permeability. Zones that are located further away tend to show either no trend or in a few cases a slight increasing trend. Zone 60-3 showed a large increase in permeability in November indicating that it may now be within the dryout region which surrounds the nearby wing heaters. This zone was noted to have a temperature above the boiling point of water.

The following zones in the 12 hydrology holes show a decreasing trend in air-permeability: 59-2, 59-3, 59-4, 60-3, 60-4, 61-2, 74-3, 76-2, 76-3, 76-4, 78-2, 78-3, 186-2 and 186-4. Zones 57-3 and 74-4 have shown an increasing trend in air-permeability. It should be noted that the boreholes 185, 57, 58, and 75, which are among the uppermost boreholes have no zones that exhibit a decreasing trend in air-permeability, indicating the limited extent of moisture being transported above the heated region. As heating continues it is expected that more of the zones closest to the wing heaters will show

increases in air-permeability as they enter the dryout region. Zones further from the heaters will start showing decreases in air-permeability as moisture is transported greater distances from the heaters.

A Comparison of Air-Permeability Results with Model Predictions

The dominant paths for gas flow will be within the high permeability fracture network due to the fact that the matrix has an intrinsic permeability that is orders of magnitude below that of the fractures and has a high liquid saturation. Because of this, we can use the fracture saturation, a parameter that is calculated within the thermal-hydrological simulations to compare with measured values of air-permeability. Figure 4.3-2 shows model simulations of saturation in the fracture system after 12 months of heating. The model simulations are discussed in more detail in "Interpretive analysis of the thermal-hydrological processes in the DST," (Tsang and Mukhopadhyay, this report). Note that the orange color visible in the upper periphery of the chart is equal to the initial pre-heat fracture saturation. The central red zone is indicative of the dryout region, surrounded by a region of increased saturation.

The match between the observed decreases in air-permeability with modeled changes in fracture liquid saturation is very good, although not exact. An examination of Figure 4.3-1 shows that the air-permeability has been measured to decline most significantly in the last three zones in boreholes 76 and 78. There is no data for 77-2 and 77-3 since the 77-3 packer is deflated. The model simulations (Figure 4.3-2) show that the last three zones in borehole 78 should be experiencing the greatest decline in air-permeability followed by significant declines in borehole 76, and a slight decrease in borehole 75. The overall agreement shows that the dominant processes of liquid transport have been captured in the model, although differences can indicate the presence of formation heterogeneity as well as the requirements for further model parameter calibration to acquired data.

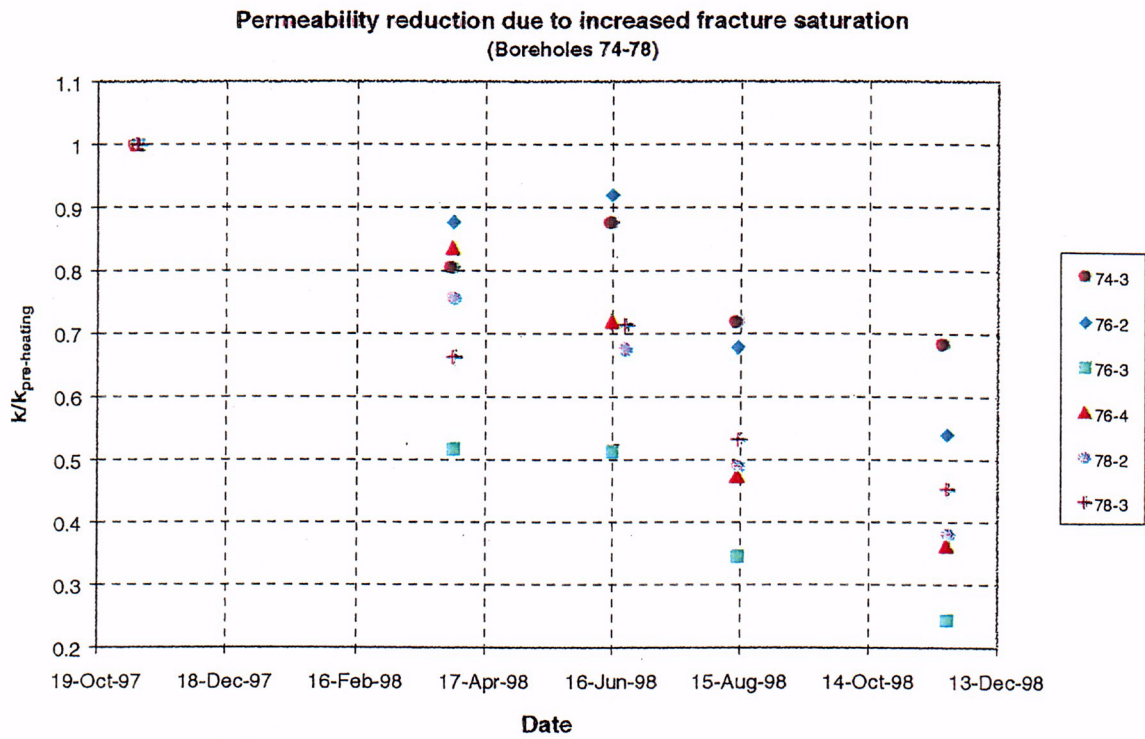


Figure 4.3-1. These intervals in the 74-78 borehole cluster have shown a consistent decrease in air-permeability as heating continues, indicating increasing liquid saturation. The zones showing the strongest decreases are located close to the heaters.

C10

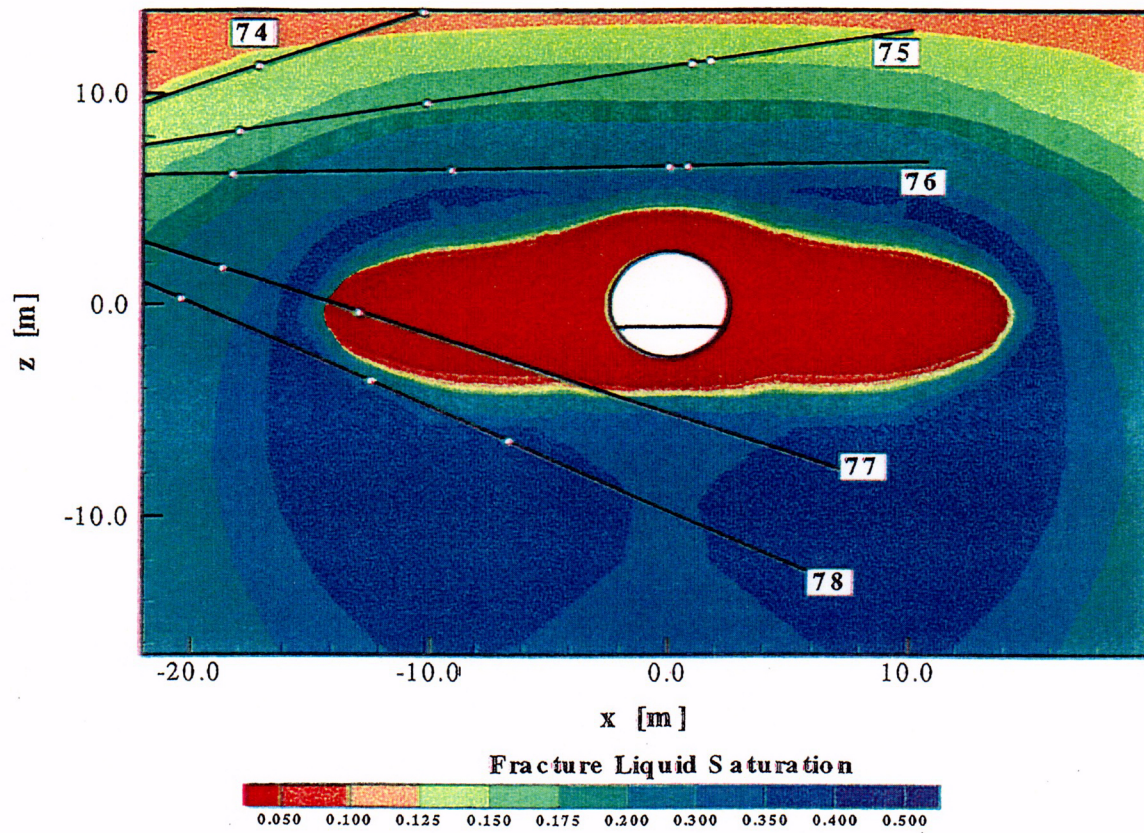


Figure 4.3-2. Simulated liquid saturation in the vertical cross-section containing the hydrology boreholes 74 -78 at 12 months of heating.

4.4 ERT Measurements

This section describes electrical resistance tomography (ERT) surveys made at the Drift Scale Test (DST), between October and December, 1998. ERT is one of the several thermal, mechanical, and hydrologic measurements being used to monitor the rock-mass response during the DST. The purpose of this work is to map the changes in moisture content caused by the heating of the rock mass water, with a special interest in the movement of condensate out of the system..

A brief synopsis of the progress made since the end of October, 1999 is presented herein. A comprehensive discussion of the process followed to produce the results shown here, equipment used, and assumptions made can be found in Wagner, 1998, pages 7-13 to 7-21.

Changes in Electrical Resistivity:

Tomographs of resistivity change corresponding to the time period between October 7, 1998, and December 9, 1998, are shown in Figures 4.4-1, 4.4-2, and 4.4-3. The top part of each of these figures shows the tomographs collected along a cross-section parallel to the Heated Drift (HD). The lower left portion of the figures shows tomographs corresponding to a vertical plane intersecting the HD at right angles, and about 5 meters in from the bulkhead; we will refer to this plane as AOD 1. The lower right portion of the figures corresponds to a second vertical plane intersecting the HD at right angles, about 24 meters in from the bulkhead; we will refer to this plane as AOD 5.

The upper part of Figure 4.4-1 shows the changes in resistivity along the HD, calculated after 308 days of heating. Note that most of the tomographs are yellow-green in color, thereby indicating resistivity ratios near 1.0 (no change relative to the pre-heat case). Near the walls of the HD, the tomographs show resistivity ratios less than 1.0, thereby indicating that the resistivity has decreased relative to the pre-heating condition. After 344 days of heating (upper portion of Figure 4.4-2), most of the rock still shows a ratio of 1.0, but the rock near the crown and invert of the HD shows stronger resistivity decreases (ratios farther removed from 1.0). These decreases become slightly stronger as heating time increases (upper portion of Figure 4.4-3). The tomographs also indicate that the resistivity changes close to the crown of the HD are stronger than those close to the invert. We believe that the resistivity changes closest to the crown and invert are due primarily to the large increases in temperature that have developed close to the walls of the HD.

The images showing resistivity changes below the HD and parallel to its axis indicate a region of anomalous resistivity decrease. This anomalous region appears as a vertical "finger" located about 17 m from the bulkhead. The resistivity decreases associated with this "finger" become stronger with time (i.e., resistivity ratio gets smaller). Also note that, as time progresses, a hole develops within the "finger" region; this hole can be clearly

observed in Figure 4.4-3. The rock within this whole showed strong resistivity decreases during the first several months of heating and now the resistivity decreases are becoming weaker as the rock becomes increasingly drier. The root cause of this behavior is described in Blair et al. (1998), pages 2-6 and 2-7, and in Figure 2-4.

The lower left portions of Figures 4.4-1, 4.4-2 and 4.4-3, shows the tomographs corresponding to AOD 1. Although the mesh consists of a large region around the electrode arrays, only the region inside the ERT electrode array is shown in the figure because the region outside the array is poorly constrained by the data. The region inside the HD is also masked because the technique does not measure rock properties in the excavated region. The tomograph sequence shows a region of resistivity decrease near the walls of the HD. The resistivity decreases become stronger with time and they extend farther into the rock above the HD. The region corresponding to the wing heaters location (nine o'clock position relative to the HD) shows relatively weak resistivity decreases.

The lower right portions of Figures 4.4-1, 4.4-2 and 4.4-3, depicts resistivity-change tomographs sampling the rock mass along AOD 5, which is a second vertical plane that intersects the HD at right angles near its middle. The images show increases (ratios greater than 1.0 near the location of the wing heaters. Resistivity decreases are observed near the walls of the HD. We suggest that the resistivity changes observed through December, 1998, are caused by temperature increases as well as saturation decreases. The AOD 5 results in Figures 4.4-1 to 4.4-3 make it clear that resistivity increases are observed in the rock closest to the wing heaters while resistivity decreases are observed farther away. This behavior is caused by the competing effects that saturation decreases and temperature increases have on electrical resistivity .

As indicated in Blair et al., 1998, for rock where temperature has increased and relatively little drying has occurred, the resistivity will decrease because the temperature increase has enhanced the mobility of the ions in the pore water. As significant drying occurs and the saturation is higher than about 30%, the pore water paths through which electrical charge moves become smaller, thereby tending to increase the bulk resistivity. However, the net change in bulk resistivity is a decrease relative to baseline because the increases in ion mobility more than compensate for the volumetric reduction of the pore water pathways. As the temperature continues to increase and the saturation drops below 30%, the pore water paths through which electrical charge moves starts to become discontinuous. This makes the bulk resistivity increase exponentially even though the increases in ion mobility caused by temperature are still present. Thus, the net effect on the bulk resistivity is an increase above baseline (i.e., the ratio becomes greater than 1.0) in hot dry rock with saturations less than 30%.

There are both similarities and differences between the AOD 1 and AOD 5 planes. Both show resistivity decreases, near the walls of the HD, that extend deeper into the rock above the crown of the HD than below its invert. A significant difference between the AOD 1 and AOD 5 results is observed in the vicinity of the wing heaters where the AOD 1 tomographs show weaker decreases in resistivity near the bulkhead while the AOD 5

tomographs show resistivity increases. Possible reasons for this difference can be found in Wagner, 1998, pages 7-13 to 7-21.

Estimates of Saturation Change:

The resistivity changes shown in Figures 4.4-1, 4.4-2, and 4.4-3 are influenced by changes in moisture content, temperature, and ionic strength of the water. To estimate saturation, it is assumed that the dominant factors affecting resistivity changes are temperature and saturation. That is, an increase in temperature or water saturation causes a resistivity decrease. Near the heaters, there may be regions where the increasing temperature reduces the resistivity, while rock drying changes the resistivity in the opposite sense (increases the resistivity). Our goal in this section is to use the images of resistivity change near the HD, along with the measured temperature field and what is known of initial conditions in the rock mass, to estimate moisture change during heating. A detailed description of this approach can be found on a previous report pertaining to the Single Heater Test (Blair et al., 1998, pages 2-5 to 2-7).

To estimate moisture content changes, the effects of both rock temperatures and resistivity changes measured by ERT must be taken into account. Interpolation of temperature measurements made at discrete points was necessary to develop the temperature fields showing temperature values at each tomograph pixel. The interpolations can sometimes be in error when the interpolation algorithm is not sufficiently constrained by the measured values and because the interpolation does not necessarily satisfy physical laws.

Note that the temperature estimates were generated following a *nonqualified* process; therefore, the saturation estimates are *nonqualified*. Also, the saturations estimates are considered approximate, as indicated later in this report.

Figures 4.4-4, 4.4-5, and 4.4-6 show the saturation change estimates corresponding to heating days 308, 344, and 371, respectively. The results shown were calculated using Model 2 as described in Blair et al., 1998, pages 2-5 to 2-7. Model 1 results are not shown in order to be concise. Note that the Model 2 estimates on Figure 4.4-4 indicate that most of the rock immediately adjacent to the HD and to the wing heaters show saturation ratios below 1.0. These estimates suggest that some drying is occurring close to the HD. A lot more drying is occurring close to the wing heaters. Also note that the drying zone is growing very slowly with time. The tomographs suggest that the drying zone extends farther into the rock above the HD and than below it. The saturation ratio estimates shown in Figure 4.4-6 suggest that the rock showing the maximum amount of drying is located in plane AOD 5, forming a horizontal zone centered on the wing heaters; also, the amount of drying higher near the AOD 5 wing heaters appears to be larger than near the AOD 1 wing heaters. The tomographs show that the rock near the AOD 5 wing heaters has lost more than four-fifths of its water (saturation ratio less than 0.20) by mid-December, 1998. When compared to AOD 1, AOD 5 shows a stronger zone of drying that extends beyond the zone where the wing heaters are located.

Saturations ratios greater than 1.0 indicate regions in the rock where water saturation is increasing relative to the pre-heating conditions; we will refer to these zones as wetting zones. Wetting zones are observed in Figures 4.4-4, 4.4-5, and 4.4-6. Most of these occur below the HD, near the bulkhead as well as in discrete zones closer to the middle of the HD. In particular, the strongest wetting zone below the HD appears to be related to the "finger" anomaly associated with figures 4.4-1, 4.4-2, and 4.4-3. Note that the "finger" resistivity anomaly correlates with a region of drying close to the HD invert, and to a region of wetting farther away from the invert. Other wetting zones appear above and near the edge of the wing heater location, within planes AOD 1 and AOD 5. Also, below and near the edge of the wing heaters in AOD 1.

All of the saturation estimates presented are considered to be approximations. The accuracy of the saturation estimates may be limited by one or more of the factors listed in Blair et al, 1998, pages 2-9 and 2-10.

References:

Blair, S., T. Buscheck, L. DeLoach, W. Lin and A. Ramirez, 1998, Single Heater Test Final Report, UCRL-ID-131491, Lawrence Livermore National Laboratory, Livermore CA; pages 2-6, 2-7, 2-9, 2-10, and Figure 2-4.

Wagner, R., 1998, Drift Scale Test Progress Report No. 1 (BAB000000-01717-5700-00004, Draft A), August 1998, TRW Environmental Safety Systems Inc., Las Vegas Nevada, pages 7-13 to 7-21.

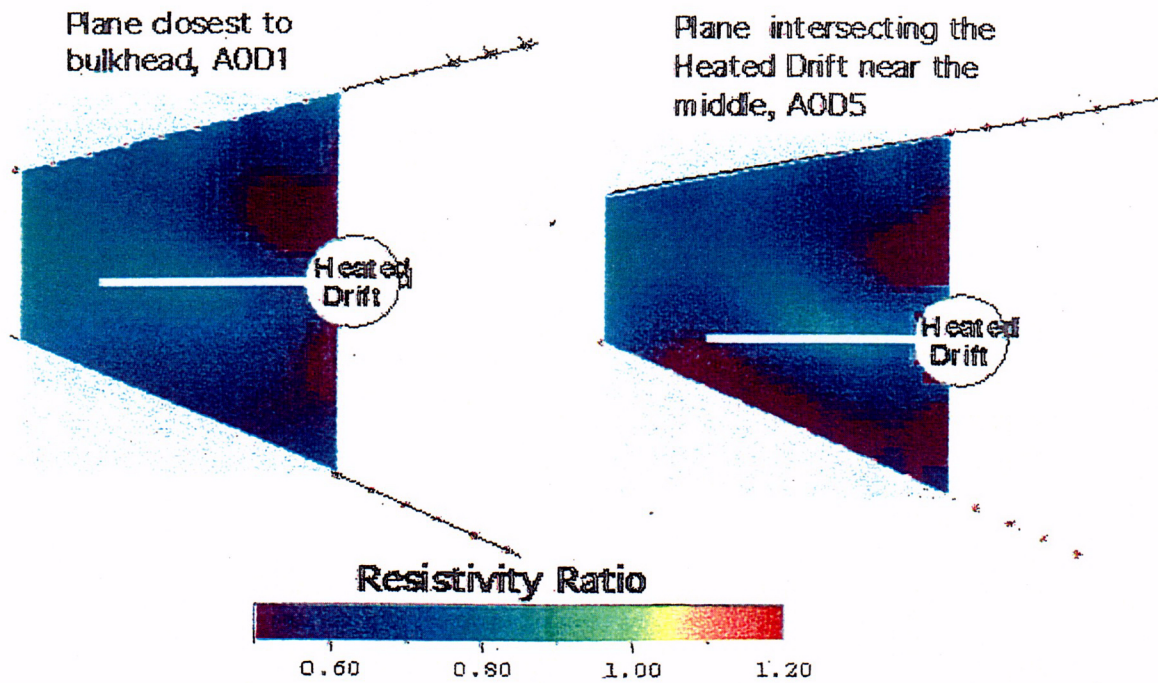
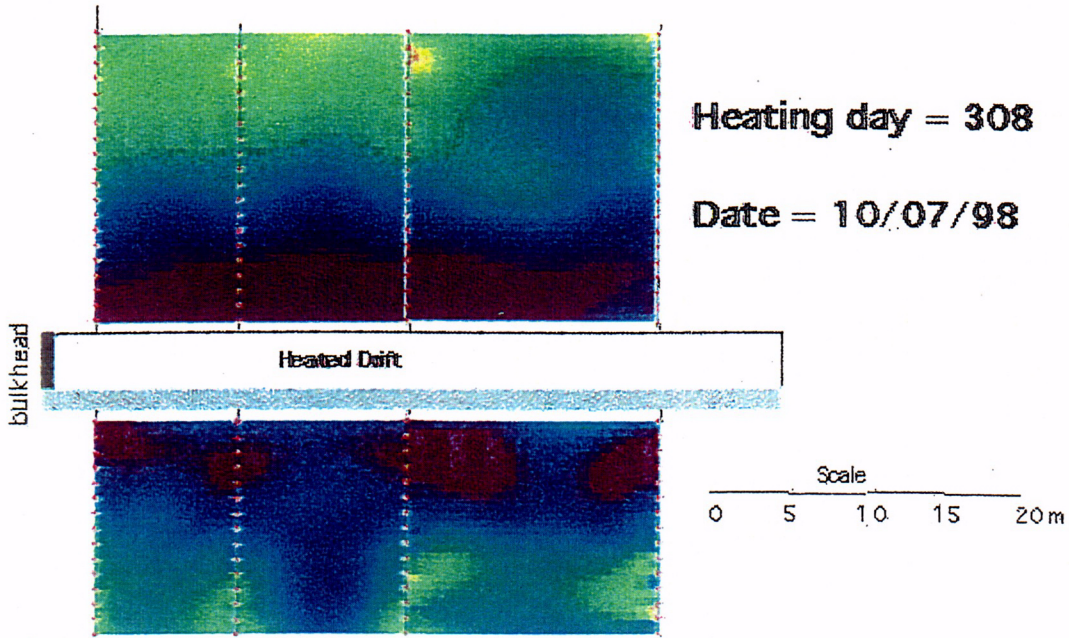


Figure 4.4-1. Tomographs of electrical resistivity ratio for heating day 308. The tomographs show changes relative to the preheating (November 18, 1997) electrical resistivity distribution. A resistivity ratio equal to 1.0 indicates no change; values less than 1.0 indicate that the resistivity is decreasing relative to the baseline. The thick white lines extending from the circle representing the HD represent the location of the wing heater boreholes.

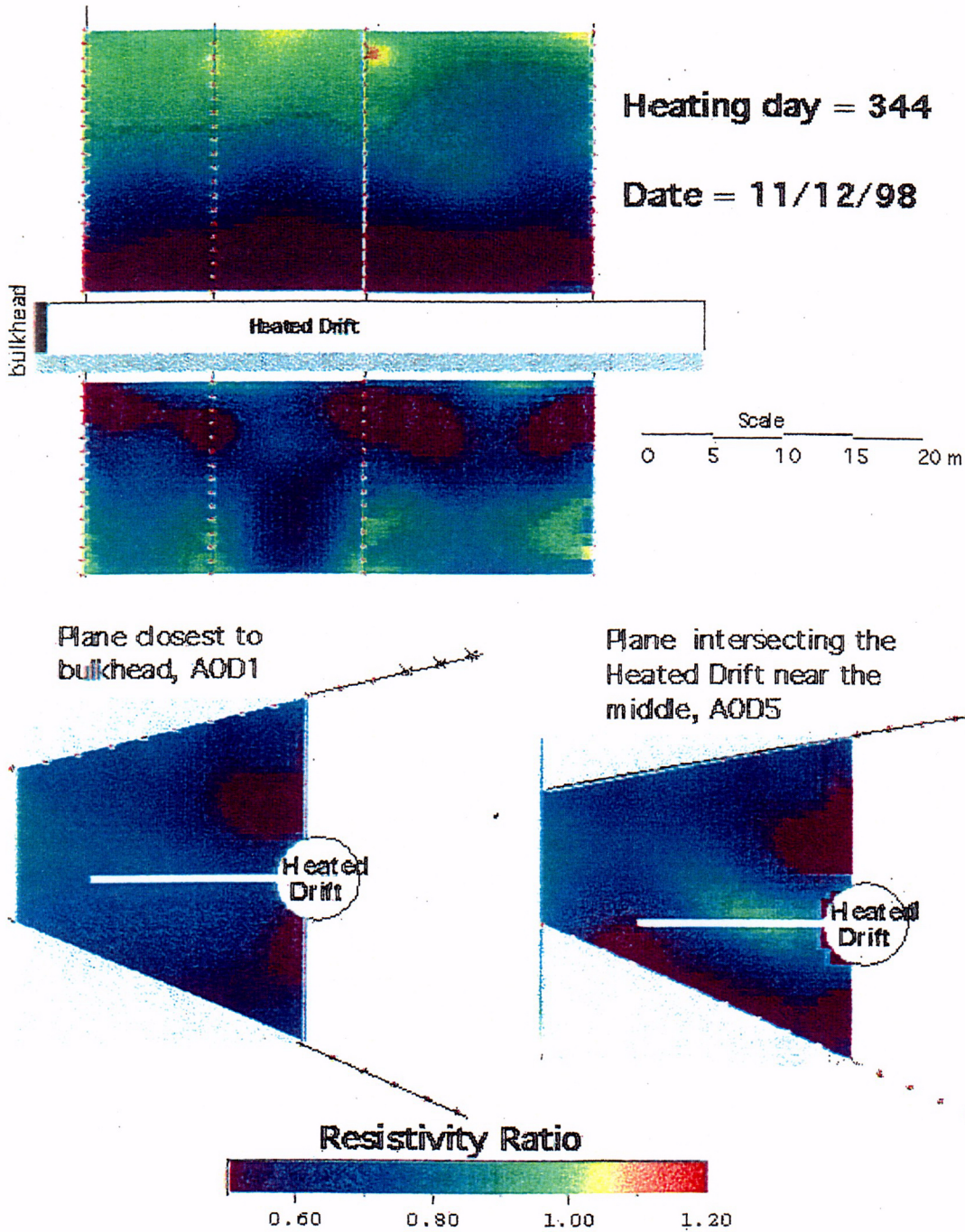


Figure 4.4-2. Tomographs of electrical resistivity ratio for heating day 344. The tomographs show changes relative to the preheating (November 18, 1997) electrical resistivity distribution. A resistivity ratio equal to 1.0 indicates no change; values less than 1.0 indicate that the resistivity is decreasing relative to the baseline. The thick white lines extending from the circle representing the HD represent the location of the wing heater boreholes.

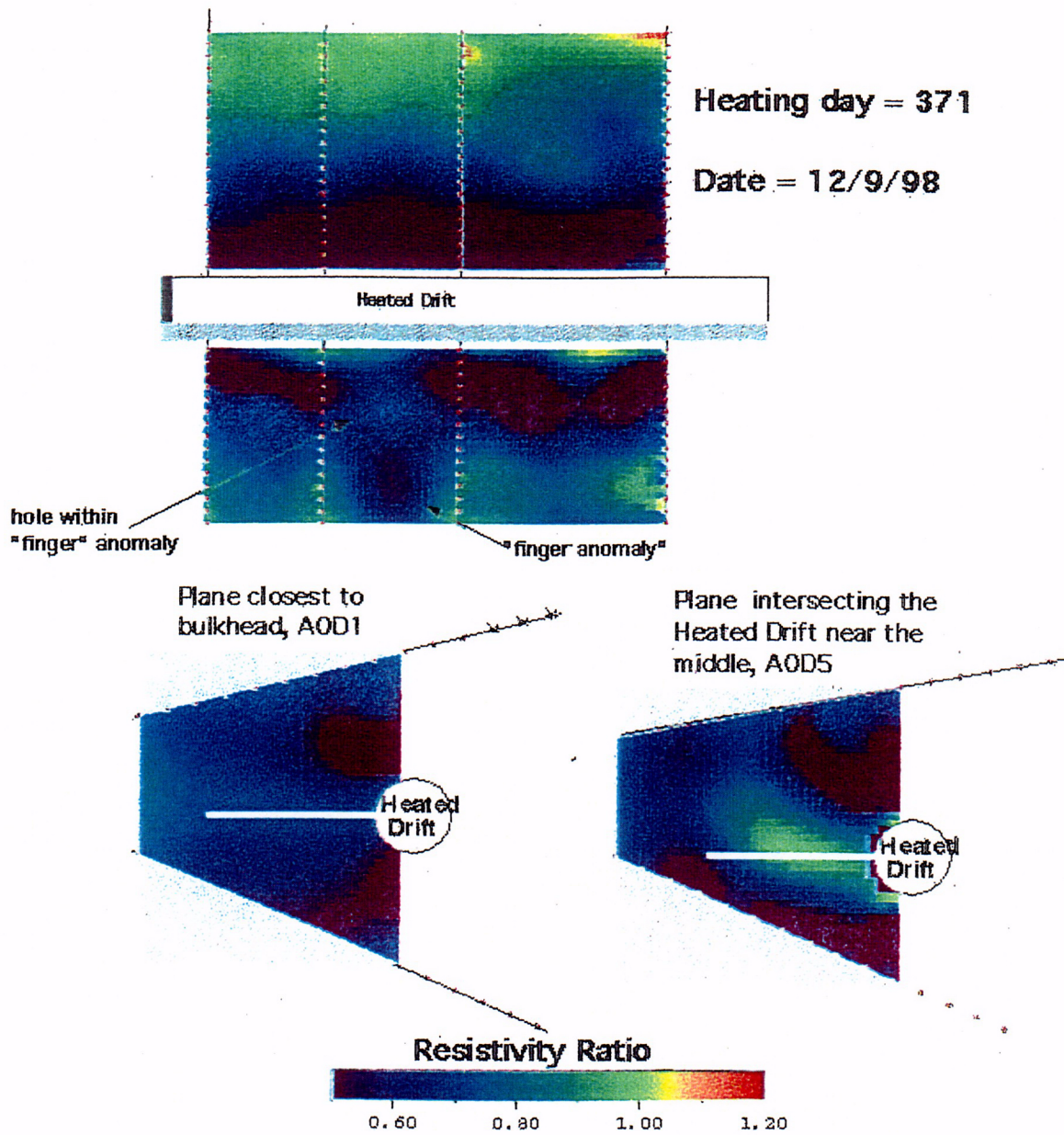


Figure 4.4-3. Tomographs of electrical resistivity ratio for heating day 371. The tomographs show changes relative to the preheating (November 18, 1997) electrical resistivity distribution. A resistivity ratio equal to 1.0 indicates no change; values less than 1.0 indicate that the resistivity is decreasing relative to the baseline. The thick white lines extending from the circle representing the HD represent the location of the wing heater boreholes.

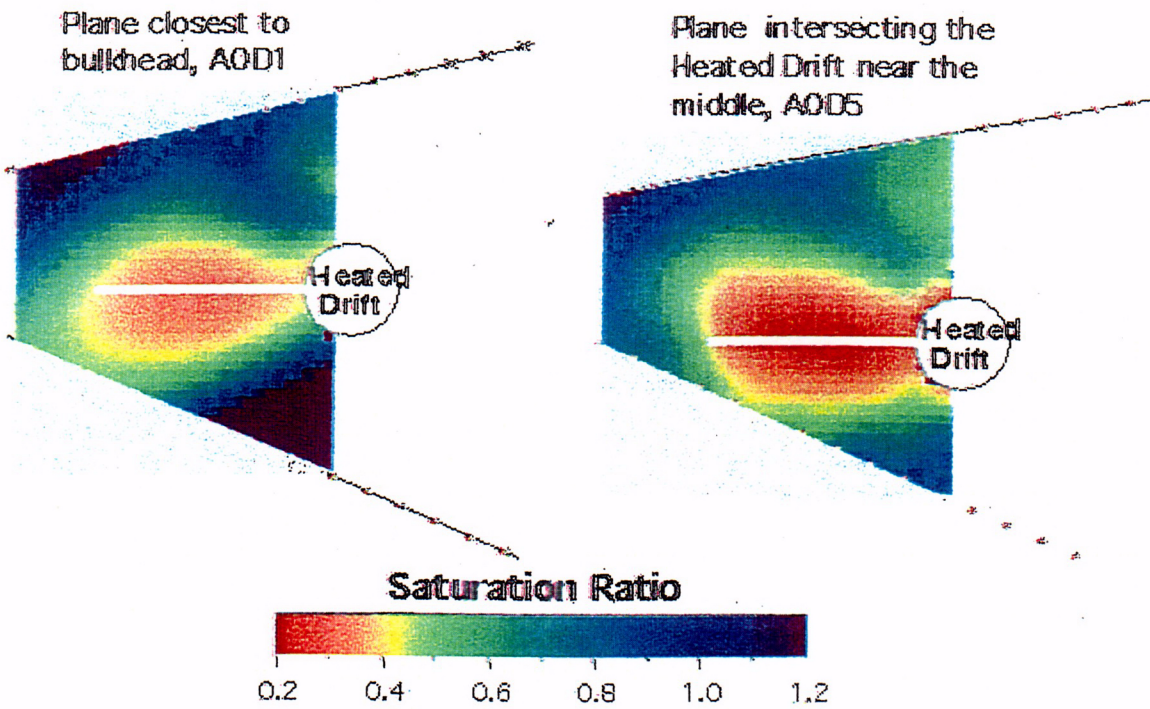
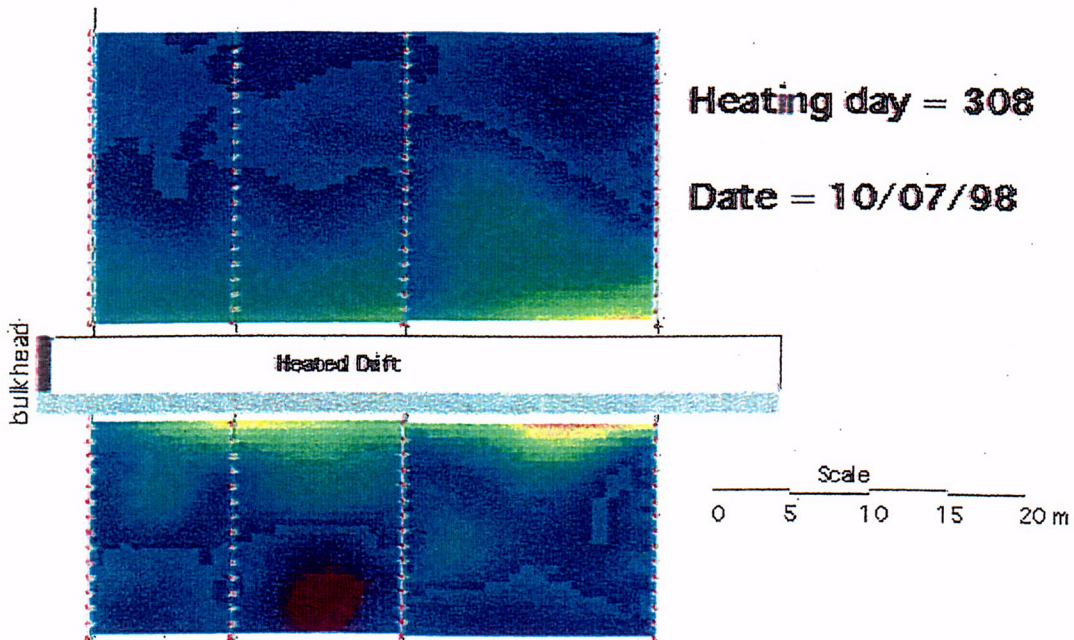


Figure 4.4-4. Tomographs of saturation ratio for heating day 308. The tomographs show changes relative to the preheating (November 18, 1997) saturation distribution. A saturation ratio equal to 1.0 indicates no change; values less than 1.0 indicate that the saturation is decreasing relative to the baseline. The thick white lines extending from the circle representing the HD represent the location of the wing heater boreholes.

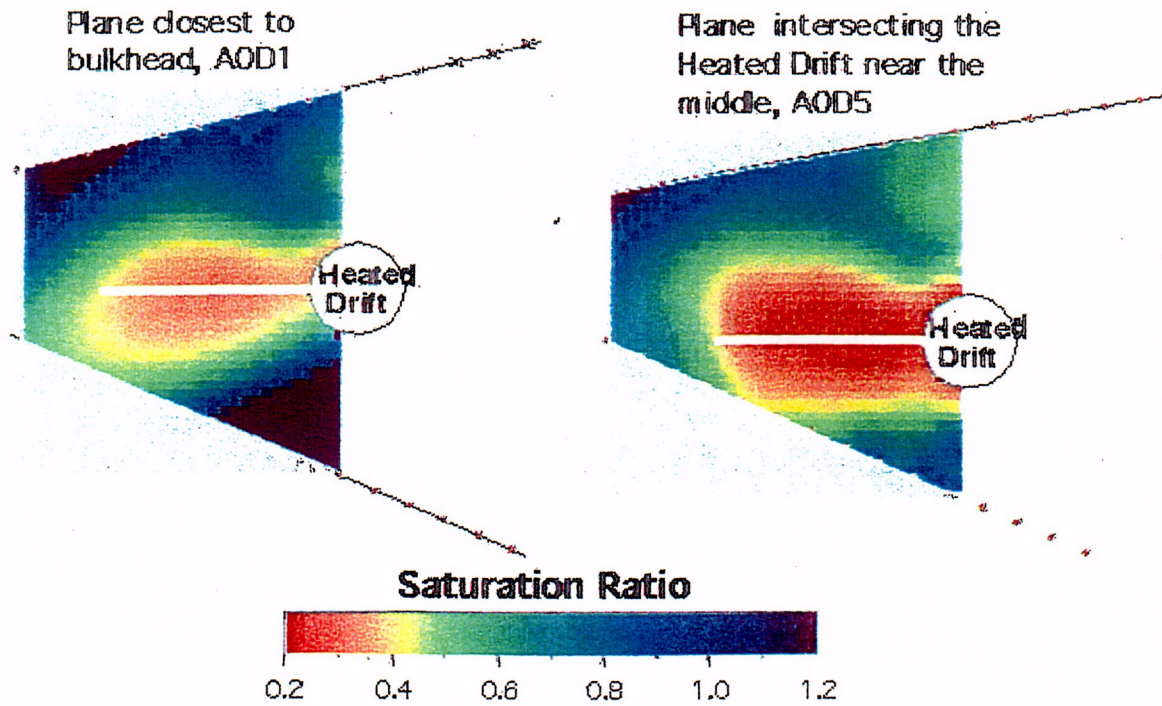
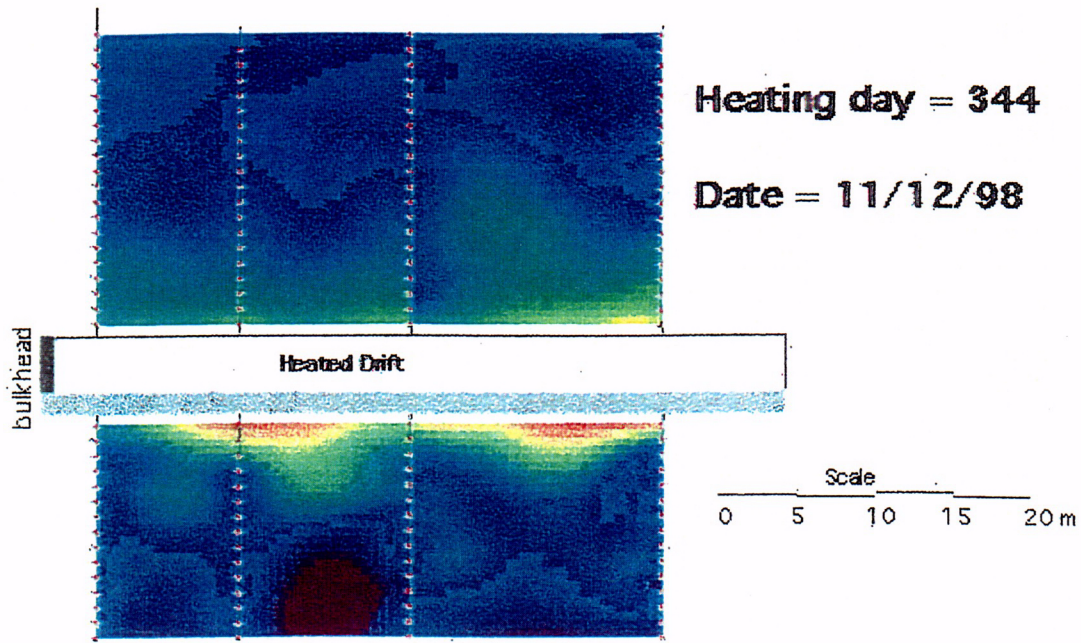


Figure 4.4-5. Tomographs of saturation ratio for heating day 344. The tomographs show changes relative to the preheating (November 18, 1997) saturation distribution. A saturation ratio equal to 1.0 indicates no change; values less than 1.0 indicate that the saturation is decreasing relative to the baseline. The thick white lines extending from the circle representing the HD represent the location of the wing heater boreholes.

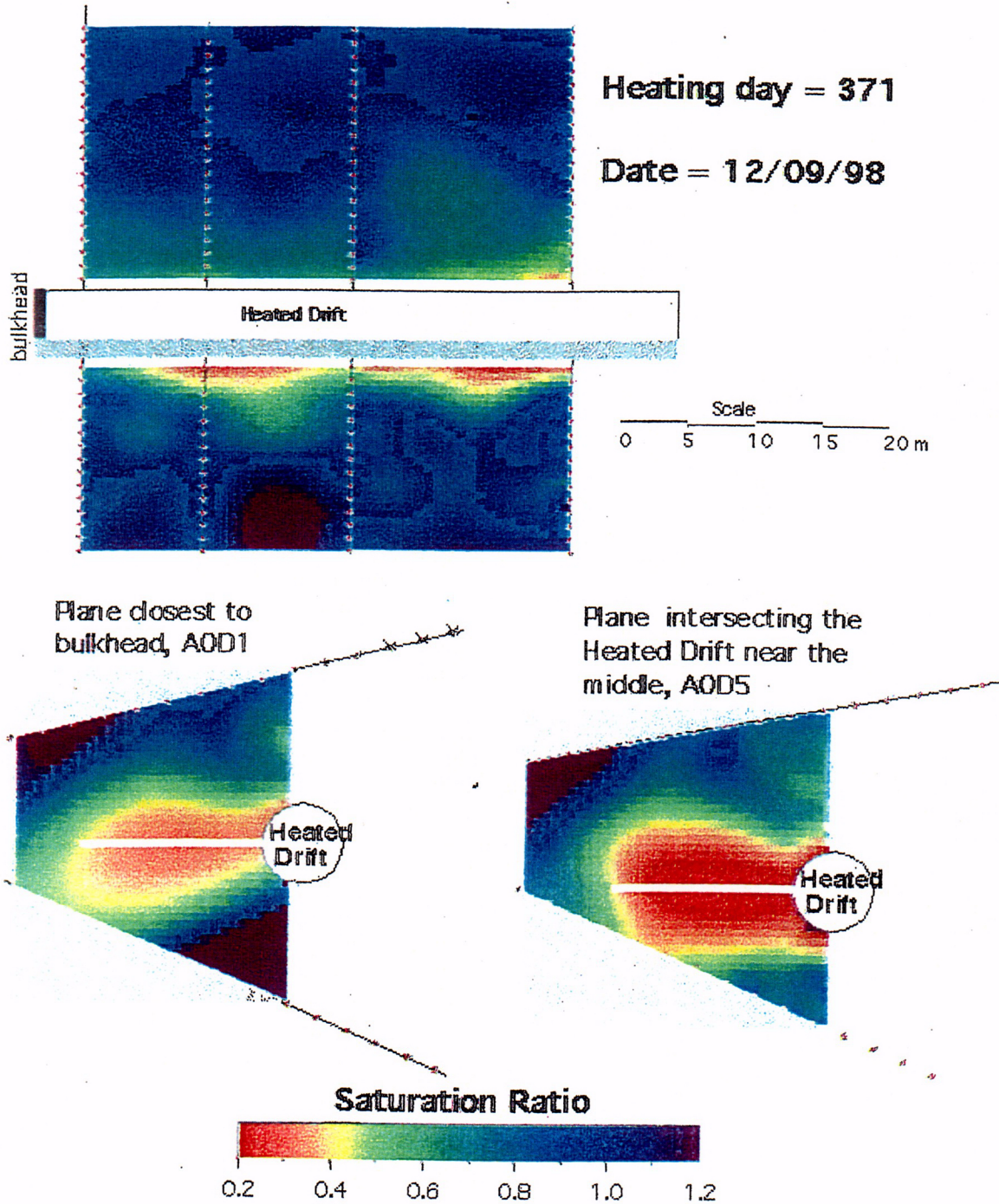


Figure 4.4-6. Tomographs of saturation ratio for heating day 371. The tomographs show changes relative to the preheating (November 18, 1997) saturation distribution. A saturation ratio equal to 1.0 indicates no change; values less than 1.0 indicate that the saturation is decreasing relative to the baseline. The thick white lines extending from the circle representing the HD represent the location of the wing heater boreholes.